

Brown carbon aerosol in rural Germany: sources, chemistry, and diurnal variations

Feng Jiang^{1,2*}, Harald Saathoff^{1*}, Junwei Song¹, Hengheng Zhang¹, Linyu Gao¹, and Thomas Leisner^{1,3}

¹Institute of Meteorology and Climate Research, Karlsruhe Institute of Technology, 76344 Eggenstein–Leopoldshafen, Germany

²Institute of Applied Geosciences, Working Group for Environmental Mineralogy and Environmental System Analysis, Karlsruhe Institute of Technology, 76131 Karlsruhe, Germany

³Institute of Environmental Physics, Heidelberg University, 69120 Heidelberg, Germany

Correspondence to: Feng Jiang (feng.jiang@kit.edu) and Harald Saathoff (harald.saathoff@kit.edu)

Abstract. Brown carbon aerosol (BrC) is one major contributor to atmospheric air pollution in Europe, especially in winter. Therefore, we studied the chemical composition, diurnal variation, and sources of BrC from 17th February to 16th March at a rural location in southwest Germany. In total, 178 potential BrC molecules (including 7 nitro aromatic compounds, NACs) were identified in the particle phase comprising on average 8363 ± 4432 ng m⁻³, and 31 potential BrC (including 4 NACs) molecules were identified in the gas phase contributing on average 8.562 ± 6.750 ng m⁻³ during the whole campaign. The 178 potential BrC molecules only accounted for $2.63 \pm 1.5\%$ of the total organic mass, but can explain $144 \pm 134\%$ of the total BrC absorption at 370 nm, assuming an average mass absorption coefficient at 370 nm (MAC₃₇₀) of 9.5 m² g⁻¹. A few BrC molecules dominated the total BrC absorption. In addition, diurnal variations show that gas phase BrC was higher at daytime and lower at night. It was mainly controlled by secondary formation (e.g. photooxidation) and particle-to-gas partitioning. Correspondingly, the particle phase BrC was lower at daytime and higher at nighttime. Secondary formation dominates the particle-phase BrC with $61 \pm 21\%$, while $39 \pm 21\%$ originated from biomass burning. Furthermore, the particle-phase BrC showed decreasing light absorption due to photochemical aging. This study extends the current understanding of real-time behaviors of brown carbon aerosol in the gas and particle phase at a location characteristic for the central Europe.

26 **1. Introduction**

27 The Brown Carbon (BrC) aerosol has significant impact on air quality and climate, since it absorbs the solar radiation
28 in the near-ultraviolet and visible region (Laskin et al., 2015; Moise et al., 2015). Global simulation showed that the
29 mean radiative forcing of BrC aerosol was -0.43 W m^{-2} and 0.05 W m^{-2} at the surface and at the top of the atmosphere,
30 accounting for 15% of total radiative forcing by the absorbing aerosol (Park et al., 2010). In addition, global
31 measurements of BrC found that the average direct radiative effect of BrC absorption accounted between 7% to 48%
32 at the top of the atmosphere (Zeng et al., 2020).

33 Some typical molecules of BrC have been identified, such as nitro-aromatic compounds (NACs), imidazoles, and
34 polycyclic aromatic hydrocarbons (PAH), etc., (Jiang et al., 2022; Wu et al., 2018; Huang et al., 2018; Liu et al., 2023).

35 In western Europe, the concentration levels of NACs range between $1\text{--}20 \text{ ng m}^{-3}$, accounting for 0.3%–4% of total
36 absorption of BrC at UV wavelengths (Jiang et al., 2022; Mohr et al., 2013; Teich et al., 2017). In addition, imidazoles
37 were detected with concentrations ranging between $0.2\text{--}14 \text{ ng m}^{-3}$ in ambient aerosol samples from different
38 environments in Europe and China (Teich et al., 2016). Furthermore, parent-PAHs and carbonyl-OPAHs accounted
39 for on average $\sim 1.7\%$ of the overall absorption of methanol-soluble BrC in Urban Xi'an, Northwest China (Huang et
40 al., 2018). Even though many studies have investigated the chemical composition of brown carbon and calculated the
41 absorption contribution from BrC molecules, there are still many unknown brown carbon molecules to allow a
42 quantitative assessment of their sources and atmospheric impact.

43 Sources of BrC can be separated as primary emissions and secondary formation. The primary sources of BrC are
44 biomass burning and fossil fuel combustion (Andreae and Gelencser, 2006). On a global scale, a majority of BrC
45 aerosol mass is associated with biomass burning dominating BrC absorption (Zeng et al., 2020). The major secondary
46 sources of brown carbon are from oxidation of aromatic volatile organic compounds, such as toluene (Lin et al., 2015),
47 naphthalene (Siemens et al., 2022), ethylbenzene (Yang et al., 2022), and indole (Montoya-Aguilera et al., 2017; Jiang
48 et al., 2023), especially in the presence of NO_2 .

49 BrC in the atmosphere can be suspended in the gas phase or particle phase. However, only a few studies have
50 investigated the sources and chemical composition of BrC in the gas phase. For example, NACs in the gas phase were
51 highest during the daytime at a rural site in China (Salvador et al., 2021). The major sources of NACs were from
52 secondary formation on days without extensive biomass burning emissions, but mainly from primary emissions in
53 biomass burning events (Salvador et al., 2021). The source of nitrophenol, a typical BrC molecule, was mainly from
54 secondary formation outweighing losses by photolysis in polluted urban environments, Beijing (Cheng et al., 2021).

55 The major chromophores of BrC in the gas phase were rich in phenol- and protein-like substances in Xi'an, China,
56 during the summer (Chen et al., 2021). Therefore, the previous studies mainly focus on sources and chromophores of
57 BrC, especially NACs. However, the real-time diurnal variation and sources of BrC in the gas phase in the atmosphere
58 have rarely been investigated in central Europe.

59 Previous field studies have investigated the sources of BrC in the particle phase which are mainly from secondary
60 formation and primary emissions (Wang et al., 2019a; Moschos et al., 2018; Satish et al., 2017). In the central Europe,
61 the secondary biogenic organic aerosol (OA) contributes less BrC in summer. However, the primary and secondary
62 wood burning emissions dominated the BrC (Moschos et al., 2018). The primary emissions of BrC contributed more
63 to organic aerosol light absorption than those from secondary processes in the North China Plain, China (Wang et al.,
64 2019a). However, secondary sources for BrC were more important for absorption than primary ones in the Southeastern
65 Margin of Tibetan Plateau (Wang et al., 2019b). Loss pathways of BrC in the particle phase mainly comprise
66 photooxidation and photobleaching, but also dilution of BrC e.g. by rising boundary layer height influences its
67 concentration levels (Satish et al., 2017; Laskin et al., 2015; Moise et al., 2015). The absorption of BrC was high in
68 the early morning and later decreased due to the bleaching of chromophores (Wang et al., 2019a; Satish et al., 2017).
69 A diurnal cycle showed that secondary chromophores can be formed from photochemical oxidation after sunrise
70 followed by photobleaching of the chromophores under the oxidizing conditions as the day progressed (Wang et al.,
71 2019b). Lower BrC concentrations during noon were explained by the fact that planetary boundary layer heights were
72 highest during the middle of the day (Liu et al., 2023). However, also nighttime aqueous-phase chemistry can promote
73 the formation of secondary light absorbing compounds and the production of strongly absorbing particles (Wang et al.,
74 2019a). In addition, higher emissions of biomass burning BrC were observed at nighttime. Actually, the BrC in the
75 particle phase undergoes complex photochemical processing during the whole day. The time dependent sources and
76 diurnal variations of BrC in aerosol particles are still reported rarely and not well understood.

77 To better understand the chemical characterization, diurnal variation, and sources of BrC in central Europe, we
78 performed online measurements of BrC during February-March 2021 at a rural location in southwest Germany. In the
79 following, we will describe the experimental methods used in this study. Subsequently, the mass concentrations of BrC
80 in gas and particle phase will be determined. Furthermore, the contribution of BrC to light absorption in the particle
81 phase will be estimated. Then, the diurnal variations and sources of BrC in the gas and particle phase will be analyzed.
82 Finally, the atmospheric implications of our findings will be discussed.

83 **2. Experimental methods**

84 **2.1. Measurement site**

85 We performed particle and trace gas measurements from February 17th–March 16th 2021 at KIT Campus Nord, a rather
86 rural area in Germany (49°05'43.1"N 8°25'45.6"E). The sampling site is located at the building number 322 of the
87 IMK-AAF on KIT Campus Nord, as shown in Figure S1. The campus is mostly surrounded by the Hardwald forest
88 dominated by pine trees. The sampling site is also near some villages e.g. 3–4 km east of the village “Eggenstein-
89 Leopoldshafen”, 6–7 km northeast of the village “Neureut”, 3–4 km west of the village “Friedrichstal”, 4–5 km
90 northwest of the village “Stutensee”, and 5–6 km southeast of the village “Linkenheim”. Therefore, influences by
91 biomass burning emissions from wood stove combustion in these residential areas during winter time can be expected
92 (Thieringer et al., 2022). Furthermore, the city of Karlsruhe with 3000000 inhabitants is 10 km south of the
93 measurement site. The city includes industrial areas with a coal-fired power plant “Rheinhafen” and a refinery “MIRO”.
94 Therefore, the measurement site is potentially affected by different aerosol sources.

95 **2.2. Meteorological, aerosol particle, and traces gas instruments**

96 All instruments were set up in a temperature-controlled measurement building. The samples were collected above the
97 roof top about 8 m above ground level via stainless steel tubes and a PM_{2.5} and a TSP inlet as well as FEP tubes for the
98 VOC measurements. An overview of the instruments used and the parameters measured is given in Table S1 of the
99 Supplement.

100 Temperature, relative humidity (RH), pressure, wind speed, wind direction, precipitation, and global radiation were
101 measured by a meteorological sensor (WS700, Lufft GmbH; see Table S1) about 8 m above the ground level. The main
102 wind directions during the campaign were southwest, northeast, and southeast, since winds were channeled by the
103 Rhine River valley. O₃ and NO₂ were measured with standard gas monitors (Table S1). The particle number
104 concentrations (>2.5 nm) were measured by a water-based condensation particle counter (CPC3789, TSI Inc.). PM_{2.5}
105 was measured by an optical particle counter (OPC-FIDAS 200, Palas Inc.). The particle number size distributions were
106 measured by a nanoparticle sizer (NanoScan, TSI Inc.) ranging from 10-410 nm at a time resolution of 1 min. Black
107 carbon (BC) concentrations were measured with aethalometers (AE33, Aerosol Magee Scientific).

108 2.3. Online FIGAERO-CIMS measurement and identifications of potential BrC molecules

109 The individual organic compounds in both the gas and particle phase were measured with a filter inlet for gases and
110 aerosols coupled to a high-resolution time-of-flight chemical ionization mass spectrometer (FIGAERO-HR-ToF-CIMS,
111 Aerodyne Research Inc. hereafter CIMS) employing iodide (I⁻) for chemical ionization (Lopez-Hilfiker et al., 2014;
112 Jiang et al., 2022). During the gas-phase measurement, the ambient air was sampled via a fluorinated ethylene
113 propylene (FEP) tube of 4.5 m length (flow rate 8 L min⁻¹, residence time 0.9 s). At the same time, the particles were
114 collected on a Teflon (Polytetrafluoroethylene, PTFE) filter via a separate sampling port connected to a PM_{2.5} inlet
115 (total flow rate 16.7 L min⁻¹) and an 8 m long stainless-steel tube. The loading time and sampling flow of Teflon filters
116 were 30 minutes and 4 L min⁻¹, respectively. At regular intervals (46 min), the gas-phase measurement was switched
117 off and particles on the filter were desorbed by a flow of ultra-high-purity nitrogen (99.9999 %) heated from room
118 temperature to 200 °C over the course of 35 min (Lopez-Hilfiker et al., 2014; Huang et al., 2019a). The resulting mass
119 spectral signal evolutions as a function of desorption temperature are termed thermograms (Lopez-Hilfiker et al., 2014).
120 Integration of thermograms of individual compounds yielded their signal in counts per second, which were converted
121 to mass concentrations using an average sensitivity of 22 count s⁻¹ ppt⁻¹ (Lopez-Hilfiker et al., 2014). After the filed
122 campaign, the calibration of 4-nitrophenol, 4-nitrocatechol, 2-methyl-4-nitrophenol, and 4-methyl-5-nitrocatechol was
123 utilized to characterize the sensitivity factor of nitro aromatic compounds (NACs), as shown in the Supplement. The
124 sensitivity factors of our iodide CIMS for 4-nitrophenol, 4-nitrocatechol, 2-methyl-4-nitrophenol, and 4-methyl-5-
125 nitrocatechol were 0.80 ± 0.44, 0.50 ± 0.32, 0.96 ± 0.52, 0.97 ± 0.63, respectively (Figure S9). The average sensitivity
126 factor of 4 NACs was 0.81 ± 0.53. We used this average sensitivity factor to calibrate other potential brown carbon
127 molecules in this study. The sensitivity factor of levoglucosan was 0.40 ± 0.14 in this study (Figure S10). We used the
128 sensitivity factor of 0.40 ± 0.14 to estimate the concentrations of molecules, which are not identified as potential BrC
129 molecules. Please note that the sensitivity of CIMS for different organic compounds varies by a few orders of
130 magnitude. Sensitivity uncertainties were taken into account in the calculation of the overall uncertainties of CIMS
131 concentrations (±60%) following the approach by Thompson et al. (2017).
132 During the measurements, the mass resolution of FIGAERO-CIMS was relatively stable with about 4000 m/Δ. The
133 interference from isomers with different vapor pressures or thermal fragmentation of larger oligomeric molecules can
134 lead to more complex, multimodal and broader thermograms (Lopez-Hilfiker et al., 2014). The signal integration can
135 include the different isomers or thermal fragmentation of larger oligomers. Therefore, the isomers or thermal

136 decomposition can lead to increase errors of estimating the organic mass concentrations. In this study, BrC molecules
137 were identified and partially quantified in atmospheric aerosol by FIGAERO-CIMS. Please note that the iodide CIMS
138 has sensitivities varying over several orders magnitude for different compounds e.g. of different oxidation states
139 (Lopez-Hilfiker et al., 2016). Therefore, the quantitative interpretation is limited to the small amount of compounds
140 for which we could do calibration with authentic standards. Keeping this in mind, it can still be meaning to a relative
141 comparison of the large number of high oxidized compounds assuming the same sensitivity. ~~In this study, atmospheric~~
142 ~~mass concentrations of BrC were detected by FIGAERO-CIMS. These values have high uncertainty with several orders~~
143 ~~of magnitude. However, this is still a reasonable method to measure the organic aerosol in atmosphere.~~ The raw data
144 were analysed by using the toolkit Tofware (v3.1.2, Tofwerk, Thun, Switzerland, and Aerodyne, Billerica) with the
145 Igor Pro software (v7.08, Wavemetrics, Portland, OR). Gas phase background was determined by sampling zero air
146 (high purity synthetic air). Particle phase backgrounds were assessed by putting an additional Teflon filter upstream of
147 the particle phase sampling port during the deposition (Huang et al., 2019a; Lee et al., 2018).

148 We observed typically about 1500 mass peaks from particles and 120 mass peaks in gases corresponding to different
149 oxygenated organic compounds by using FIGAERO-CIMS. Individual compounds were assigned to the mass peaks
150 by fitting, $C_cH_hO_oN_n$, different numbers of atoms: c carbon, h hydrogen, o oxygen, n nitrogen (Lopez-Hilfiker et al.,
151 2014). A double bond equivalent (DBE) can be calculated as follows (Daumit et al., 2013):

$$152 \quad DBE = \frac{n-h}{2} + c + 1 \quad (1)$$

153 Lin et al., (2016, 2018) employed high-resolution mass spectrometry to analyze biomass burning organic aerosol. They
154 assigned potential brown carbon compounds according to the correlation of double bond equivalents (DBE) with the
155 number of carbon atoms per molecule (Figure S12). We used this method to assign 178 potential BrC molecules
156 (including 7 NACs) in the particle phase and 31 potential BrC molecules (including 4 NACs) in the gas phase, as
157 shown in Figure 1 in the corresponding mass spectra. The gas to particle phase partitioning coefficients of those semi
158 volatile potential brown carbon molecules which could be measured in both phases with sufficient sensitivity are listed
159 in table S6. A few other studies used this method also to assign more brown carbon molecules. For example, good
160 correlations ($r = 0.9$) between mass absorption efficiency at 365 nm and potential brown carbon molecules of larger
161 molecular weight were found by Tang et al., (2020). Xu et al., (2020) used this method to assign 149 nitrogen-
162 containing potential BrC chromophores at the Tibetan Plateau and we used this method to assign potential BrC
163 molecules in downtown Karlsruhe (Jiang et al., 2022). The potential BrC molecules we assigned according to this

164 ~~method for the particle and the gas phase are listed in Tables S2 and S3. Lin et al. (2018) assigned potential brown~~
165 ~~carbon compounds in the plot of DBE vs the number of carbon atoms per molecule. They employed high resolution~~
166 ~~mass spectrometry to analyze biomass burning organic aerosol. We used this method to find potential BrC molecules~~
167 ~~(Jiang et al., 2022). The potential BrC molecules in the particle and gas phase were shown in Table S2 and S3.~~

169 **2.4. Particle light absorption from aethalometer measurements**

170 In the aethalometer AE33 (Magee Scientific), aerosol particles are continually sampled on a quartz filter and the optical
171 attenuation is measured with time resolutions 1 minute at seven wavelengths (370, 470, 520, 590, 660, 880, and 950
172 nm) during this campaign. The light absorption at seven wavelengths was calculated from the measured attenuation.
173 Attenuation is measured on two spots with different sample flows and on the reference spot without sample flow. The
174 two loading spots with different flow are used to allow for loading effect corrections (Drinovec et al., 2015). ~~Since~~
175 ~~our aethalometer has been used two loading spots, the loading effect was corrected by a Dual-spot loading~~
176 ~~compensation algorithm (Drinovec et al., 2015). To further address the scattering effect (Yus-Díez et al., 2021), we~~
177 ~~did comparison experiments in the Aerosol Preparation and Characterization (APC) chamber (Huang et al., 2018).~~
178 ~~Black carbon was injected into the APC chamber by using the PALAS soot generator (GfG 1000, Palas) (Saathoff et~~
179 ~~al., 2003). The APC chamber was connected to a photoacoustic spectrometer (PAS) operating at three wavelengths~~
180 ~~(405, 520, and 658 nm) (Linke et al., 2016) and an aethalometer AE33. As shown in Figure S11, for three wavelengths~~
181 ~~(370, 520, and 660 nm), the correlation slopes were 1.88, 1.94, and 1.98, respectively. The average multiple-scattering~~
182 ~~correction factor was 1.90 ± 0.06 in this study. The light absorption of aerosol particles on the filter is also influenced~~
183 ~~by scattering of light within filter which will enhance the light absorption. In this measurement, we used the default~~
184 ~~value (1.57) to do the scattering correction (Drinovec et al., 2015).~~

185 The BC mass concentration is calculated from the change in optical attenuation at 880 nm in the selected time interval
186 using the mass absorption cross section $7.77 \text{ m}^2 \text{ g}^{-1}$ (Gundel et al., 1984), since other aerosol particles (organic aerosol
187 or mineral) have less absorption at this wavelength and major absorption is contributed from BC alone. The attenuation
188 mass absorption coefficients of AE33 from 370 – 880nm were 18.47, 14.54, 13.14, 11.58, 10.35, and $7.77 \text{ m}^2 \text{ g}^{-1}$,
189 respectively. ~~The absorption measurements by aethalometer have the filter-based lensing effect (Moschos et al. 2021).~~
190 ~~According to previous studies, the uncertainty from lensing effect for BC and BrC measurement were 8%-27% and~~
191 ~~6%-20%, respectively (Moschos et al. 2021). We assumed an AAE_{BC} value of 1.0 in this study. However, this~~

192 assumption introduces an uncertainty in the estimations of BC and BrC light absorptions. According to previous studies,
 193 the AAE_{BC} ranges between 0.8-1.4 (Lack and Langridge 2013). This range although maybe not fully applicable to our
 194 measurement location, potentially causes relatively large uncertainties of up 81% (at 370nm) in splitting between BrC
 195 and BC absorption (Figure S13) (Duan et al. 2024). Despite these potentially large uncertainties on absolute absorption
 196 values, we consider this method still useful. Our assumption of $AAE_{BC} = 1.0$ is reasonable for our location as based on
 197 previous measurements and it should still allow to discuss the relative evolution of BC and BrC absorption.

198 We assumed that the absorption from dust and other aerosol was negligible. Hence, the absorption was only
 199 contributed from BC and BrC. Therefore, $Abs(\lambda)$ can be divided in BC and BrC absorption:

$$200 \quad Abs = Abs_{BrC}(\lambda) + Abs_{BC}(\lambda) \quad (2)$$

201 where $Abs_{BrC}(\lambda)$ is the absorption caused by BrC at the following aethalometer wavelengths, $\lambda = 370, 470, 520, 590,$
 202 or 660 nm while $Abs_{BC}(\lambda)$ is the absorption contributed by BC at the same wavelength (Wang et al., 2019). To
 203 determine $Abs_{BC}(\lambda)$ at each wavelength, we assumed that BC was the only absorber at $\lambda = 880$ nm, and thus the $Abs_{BC}(\lambda)$
 204 ($\lambda = 370, 470, 520, 590,$ and 660) can be extrapolated from the following equation:

$$205 \quad Abs_{BC}(\lambda) = Abs_{880} \times \left(\frac{\lambda}{880}\right)^{-AAE_{BC}} \quad (3)$$

206 where AAE_{BC} represents the spectral dependence of $Abs_{BC}(\lambda)$, and a value of 1.0 was chosen for AAE_{BC} based on
 207 previous studies in Germany (Teich et al., 2017). Finally, one can obtain the $Abs_{BrC}(\lambda)$ as follows:

$$208 \quad Abs_{BrC}(\lambda) = Abs(\lambda) - Abs(880) \times \left(\frac{\lambda}{880}\right)^{-AAE_{BC}} \quad (4)$$

209
 210
 211 ~~We assumed negligible absorption by dust and thus, Abs_{λ} can be divided into BC and BrC absorption. Therefore, the~~
 212 ~~$Abs_{BrC}(\lambda)$ can be calculated as follows:~~

$$213 \quad Abs_{BrC}(\lambda) = Abs(\lambda) - Abs(880) \times \left(\frac{\lambda}{880}\right)^{-AAE_{BC}} \quad (2)$$

214 ~~Where $Abs_{BrC}(\lambda)$ is the absorption caused by BrC at $\lambda = 370, 470, 520, 590,$ or 660 nm, the $Abs(\lambda)$ is total absorption~~
 215 ~~by AE33, the $Abs(880)$ is the light absorption at 880 nm, and the AAE_{BC} is 1.~~

216 The fraction of wood burning black carbon (BC_{wb}) was calculated by using the Aethalometer model (Sandradewi et
 217 al., 2008a; Sandradewi et al., 2008b):

$$218 \quad BC_{wb} = \left[\frac{b_{abs}(470nm) - b_{abs}(950nm) \times \left(\frac{470}{950}\right)^{-aff}}{\left(\frac{470}{950}\right)^{-awb} - \left(\frac{470}{950}\right)^{-aff}} \right] / b_{abs}(950nm) * BC \quad (35)$$

219 Where two pairs of Ångström exponents values were utilized to obtain BC associated with fossil fuel (BC_{ff}) and wood
220 burning (BC_{wb}). One of the largest sources of uncertainty in the Aethalometer model is related to the section of α_{ff} and
221 α_{wb} values (Healy et al., 2017; Zotter et al., 2017). In addition, the α_{ff} was typically in the range of $\sim 0.8 - 1.2$ in
222 ambient air whereas α_{wb} can vary from 1.6 to 2.2 (Saarikoski et al., 2021). However, we used the α_{ff} and α_{wb} values
223 as 0.95 and 1.68 to calculate the BC source (Helin et al., 2018), since our measurement site is in a rural area and nearby
224 a suburban area. \therefore α_{ff} and α_{wb} of 0.95 and 1.60 were applied (Saarikoski et al., 2021).
225

226 3. RESULTS AND DISCUSSION

227 3.1. Overview of the field observations

228 Figures S1 and S2 give an overview of the measurement location and the meteorological parameters, traces gases,
229 particle concentrations, and their optical properties during the campaign. The major wind directions at KIT Campus
230 Nord, 3 km east of the village of Eggenstein-Leopoldshafen, were northeast and southwest (Figure S1) caused by
231 channeling of the wind in the Rhine valley. The average wind speeds were 1.1 ± 0.8 (average \pm standard deviation) m
232 s^{-1} . Depending on meteorological conditions, local sources and regional transport had a major impact on air quality in
233 Leopoldshafen in summer (Shen et al., 2019). As shown in Figure S1 and S5, O_3 had diurnal variations with peaks at
234 daytime and an average of $41.3 \pm 26.2 \mu g m^{-3}$ during the campaign. In contrast, the relative humidity (RH) showed
235 diurnal variations with peaks at nighttime and an average of $68 \pm 16\%$ during the campaign (Figure S5). The average
236 temperature during the winter campaign was $6.5 \pm 5.6 \text{ }^\circ C$ and slowly increased from beginning to the end of the
237 campaign. NO_2 had high concentrations at some periods e.g. from 20th to 23th February with $22 \pm 8.6 \mu g m^{-3}$ and from
238 2nd to 4th March with $35 \pm 14 \mu g m^{-3}$. The average SO_2 concentration was $0.8 \pm 1.0 \mu g m^{-3}$, significantly lower than the
239 NO_2 concentrations. During some Saharan dust events, the $PM_{2.5}$ and PM_{10} mass concentrations were 21 ± 6 and $45 \pm$
240 $20 \mu g m^{-3}$, respectively, from 18th to 26th February and 19 ± 6 and $24 \pm 7 \mu g m^{-3}$, respectively, from 1st to 4th March as
241 indicated by red boxes in the lowest panel of Figure S1+S2. In addition, BC showed many spikes and a good correlation
242 ($r^2 = 0.8$) with NO_2 (Figure S2+S3). This indicates that there were many combustion events during the campaign (Figure
243 S3). The absorption Ångström exponents of particles between 370 and 520 nm ($AAE_{370-520}$) and $AAE_{660-950}$ had diurnal
244 variations with peaks at nighttime. We calculated the fraction of wood burning BC and fossil fuel BC as shown in
245 Figure S2-S3 using the Aethalometer model (Sandradewi et al., 2008a). During the winter campaign, the biomass

246 burning BC was on average $0.6173 \pm 0.0496 \mu\text{g m}^{-3}$, mostly higher than $0.3-0.25 \pm 0.273 \mu\text{g m}^{-3}$ for fossil fuel BC.
247 The $\text{AAE}_{370-520}$, $\text{AAE}_{660-950}$, biomass burning BC, and NO_2 values were enhanced from 20th to 23th February and 2nd to
248 4th March. This indicates that strong biomass burning (BB) events were on these days. During this winter campaign,
249 the BrC absorption accounted for ~40% of total absorption caused by BC and BrC at 370 nm. This points to the at least
250 regional or seasonal importance of BrC absorption which has an important effect on air quality and climate.

251 3.2. Mass concentrations and volatility of potential brown carbon molecules

252 Figure ~~1-2~~ shows an overview of levoglucosan concentrations, BC concentrations, absorption of brown carbon at 370
253 nm ($b_{\text{BrC}370}$), $\text{AAE}_{370-520}$, volatility and mass concentrations of 178 potential brown carbon molecules identified in the
254 particle phase and 31 potential brown carbon molecules in the gas phase during the whole winter campaign. We
255 identified 178 potential BrC molecules according to the method developed by Lin et al., (2018) (cf. section 2.3.). The
256 mass of these molecules shows a good correlation ($r=0.7 \pm 0.1$) with the absorption at 370 nm ($b_{\text{BrC}370}$) of BrC (sf.
257 Figure S6). We identified 178 BrC molecules showing a good correlation ($R=0.8$) with the absorption at 370 nm (abs_{370})
258 of BrC (Figure S6). This indicates that it is meaningful to extract these 178 potential BrC molecules from more than
259 one thousand and five hundred molecules detected by FIGAERO-CIMS based on the double bond equivalent/carbon
260 number ratio (DBE/C) of each molecule being higher than 0.5 and less than 0.9. The levoglucosan showed a good
261 correlation ($r = 0.7$) with BC. This is in line with the large fraction of biomass burning contributing to BC during the
262 winter campaign. Biomass burning BC accounted for (71 ± 40)% of total BC as we discussed above. The levoglucosan
263 had a good correlation ($r=0.7$) with BC. This also indicates that BC was mainly emitted from biomass burning during
264 the winter campaign. Consistently, biomass burning BC accounted for 70% of total BC as we discussed above. The
265 178 potential BrC molecules detected in the particle phase correspond to an average mass concentrations of ~~8363~~ \pm
266 ~~4432~~ ng m^{-3} . In addition, the nitro aromatic compounds (NACs) were also detected during the winter campaign. The
267 mass concentration of $\sum\text{NACs}$ in the gas phase and particle phase were $1.92 \pm 1.50.9 \text{ ng m}^{-3}$ and $17.5-40.7 \pm 18.410.7$
268 ng m^{-3} , respectively (Table S4 and S5). Mohr et al. (2013) found that five BrC molecules (nitro aromatic compounds)
269 were 20 ng m^{-3} detected by CIMS during winter in Detling, United Kingdom. Jiang et al. (2022) measured an average
270 concentration of five BrC molecules (nitro aromatic compounds) of $1.6 \pm 0.9 \text{ ng m}^{-3}$ during the winter at a kerbside in
271 downtown Karlsruhe, a city in southwest Germany and close to our measurement site. Therefore, the detection of the
272 178 potential-BrC molecules allows more complete assessment of the BrC concentrations during this winter campaign.
273 Their concentrations were significantly higher for biomass burning (BB) events e.g. $14403 \pm 4134 \text{ ng m}^{-3}$ at BB event

274 1 and 12402 ± 3934 ng m⁻³ at BB event 2, respectively. In addition, the absorption of brown carbon at 370 nm ($b_{\text{brC}370}$)
275 had high peaks with ~ 100 Mm⁻¹ and the AAE₃₇₀₋₅₂₀ of particles increased from ~ 1.5 to ~ 2 during the BB events. The
276 average concentration of potential BrC in the gas phase was $8.56.2 \pm 6.75.0$ ng m⁻³ during the winter campaign. At BB
277 events, their concentration can reach up to 3826 ng m⁻³. Therefore, biomass burning had a significant impact on optical
278 properties of aerosol and brown carbon concentrations. The lowermost panel of Figure 4.2 shows the temporal variation
279 of the average volatility of brown carbon molecules in the gas and particle phase. The average volatility or saturation
280 concentration ($\log_{10}C_{\text{sat}}$) of potential BrC in the particle phase was with -1.1 ± 0.5 $\mu\text{g m}^{-3}$ lower than 0.9 ± 0.6 $\mu\text{g m}^{-3}$
281 of potential BrC in the gas phase during the winter campaign. Organic compounds with $\log_{10}C_{\text{sat}}$ lower than -4.5 $\mu\text{g m}^{-3}$,
282 between -4.5 and -0.5 $\mu\text{g m}^{-3}$, between -0.5 and 2.5 $\mu\text{g m}^{-3}$, and between 2.5 and 6.5 $\mu\text{g m}^{-3}$ are termed extremely low-
283 volatility organic compounds (ELVOCs), low-volatility organic compounds (LVOCs), semi-volatile organic
284 compounds (SVOCs), and intermediate-volatility organic compounds (IVOCs), respectively (Donahue et al., 2009).
285 Therefore, BrC in the particle phase can be classified on average to the LVOCs and BrC in the gas phase to the SVOCs.

286 3.3 Absorption contribution of nitroaromatic compounds and potential brown carbon molecules

287 Black carbon dominated light absorption of aerosol particles with a contribution of 100% at 880 nm and decreasing to
288 73% at 370 nm. With shorter wavelengths, the brown carbon absorption contribution significantly increased
289 contributing 27% of total aerosol absorption at 370 nm (Figure 2a3a). We have no independent quantification of the
290 total organic aerosol mass loadings. However, we estimated the total organic mass as a fraction of 50 ± 20 % of $\text{PM}_{2.5}$
291 which is a typical fraction for at the location (Song et al., 2022; Song et al., 2024). According to this assumption, the
292 average organic mass concentration was 4.5 ± 3.1 $\mu\text{g m}^{-3}$. The organic mass detected by FIGAERO-CIMS based on
293 calibrated sensitivity factors was 37 ± 20 % of the estimated organic mass. This is in a similar range as observed in
294 previous studies (Ye et al., 2021). Since the online instrument to measure total organic aerosol mass, the AMS, wasn't
295 available during this campaign, we estimated the total organic mass as a fraction of 40% of $\text{PM}_{2.5}$ which is a typical
296 fraction for this season and region (Song et al., 2022; Huang et al., 2019b). Based on this assumption, the average
297 organic aerosol mass concentration calculates to 4.2 ± 3.0 $\mu\text{g m}^{-3}$. We calculated the light absorption of NACs by using
298 molecular MAC₃₆₅ (Xie et al., 2017), as shown in Table S5. Based on this, the mean light absorption of the sum of the
299 seven NACs was calculated to be 0.24 ± 0.12 Mm⁻¹, contributing to $2.24.3 \pm 2.14.4$ % of total BrC absorption at 370
300 nm, but they only contributed 0.4534 ± 0.32 % of the total organic mass.

301 In order to calculate the light absorption from the other 171 potential brown carbon molecules identified, we assumed
302 an average MAC value of $9.5 \text{ m}^2 \text{ g}^{-1}$ at 370 nm for all BrC molecules to estimate their absorption (Jiang et al., 2022).
303 So far, the MAC_{370} of most potential brown carbon molecules are still unknown. In addition, since the potential BrC
304 molecules detected by FIGAERO-CIMS could have isomers effect, we did not calibrate mass absorption coefficients
305 of 171 potential BrC. Despite these uncertainties, we think it is reasonable to estimate the order magnitude of the total
306 BrC absorption based on this assumption. Therefore, it could have uncertainty to estimate the absorption of total BrC
307 absorption based on this assumption. However, it is still a reasonable method to estimate the BrC absorption. Based on
308 this assumption, we calculated the light absorption of the 171 potential brown carbon molecules identified to $0.65 \pm$
309 0.3 Mm^{-1} at 370 nm as average for the whole winter campaign. This is half the values Jiang et al. (2022) found as mean
310 light absorption of 316 potential BrC molecules of $1.2 \pm 0.2 \text{ Mm}^{-1}$ at 365 nm for downtown Karlsruhe in winter.
311 Relative to this total organic aerosol particle mass and the measured brown carbon absorption, the 171 potential
312 identified brown carbon molecules and 7 NACs only accounted for $2.63 \pm 1.5\%$ of the total organic mass, but explain
313 $144 \pm 134\%$ of total brown carbon absorption at 370 nm (Figure 2b-3b and 2e3c). Palm et al. (2020) found that
314 particulate nitroaromatic compounds (BrC molecules) can explain $29 \pm 15\%$ of average BrC light absorption at 405
315 nm, despite accounting for just $4 \pm 2\%$ of average OA mass in fresh wildfire plumes. Mohr et al. (2013) found that five
316 nitroaromatic compounds (BrC molecules) are potentially important contributors to absorption at 370 nm measured by
317 an aethalometer and account for $4 \pm 2\%$ of UV light absorption by brown carbon in Detling, United Kingdom during
318 winter. Jiang et al. (2022) determined a mean light absorption of the 316 potential BrC molecules accounting for $32 \pm$
319 15% of methanol-soluble BrC absorption at 365nm, but only accounted for $2.5 \pm 0.6\%$ of the organic aerosol mass.
320 Therefore, even small mass fractions of strongly absorbing brown carbon molecules can dominate the brown carbon
321 absorption.

322 **3.4 Diurnal variations and sources of potential BrC in the gas phase**

323 As shown in Figure 3a4a, the 31 gas-phase potential BrC (GBrC) molecules showed higher concentrations at daytime
324 (09:00-17:00) and lower concentration between evening and early morning (18:00-08:00). Salvador et al. (2021) also
325 found that 16 gas-phase nitro-aromatic compounds (BrC molecules) measured by FIGAERO-CIMS were higher during
326 daytime and lower at nighttime during winter in rural China. As discussed above, strong biomass burning emission
327 were mostly observed at evening and early morning hours. However, gas-phase BrC had no peaks during those time
328 periods. Therefore, the primary emission from biomass burning was not a major source for GBrC at KIT Campus Nord.

329 It seems to be mainly controlled by secondary formation (e.g. photochemical smog) or/and particle-to-gas partitioning
330 (Salvador et al., 2021).

331 To demonstrate how secondary formation and partitioning control the gas-phase BrC in rural Germany, we plotted
332 diurnal profiles of the average volatility and volatility fractions of IVOC, SVOC, and LVOC of the gas-phase BrC
333 (Figure 3b4b). The LVOC of BrC increased at evenings and decreased at daytime. In contrast, the IVOC of BrC
334 increased at daytime and reached ~17% of total $\log_{10}C^*$ (volatility) in gas-phase BrC while SVOC remained with a
335 relative constant fraction (~60%). Furthermore, the IVOC fraction of BrC in the particle-phase was only 1.5% with a
336 flat diurnal profile (Figure S7). The O/C ratio of gas-phase BrC also increased during daytime (Figure 3d4d). Therefore,
337 the higher fraction of IVOC in the gas phase at daytime is most likely caused by secondary formation e.g.
338 photochemical conversion/aging because of higher oxidant levels as indicated e.g. by higher concentration of ozone at
339 same time (Figure 4c) (Saarikoski et al., 2021). Therefore, the higher fraction of IVOC in the gas phase at daytime
340 could be mainly caused by secondary formation e.g. photochemical aging because of higher concentrations of O₃ at
341 same time (Figure 3c) (Salvador et al., 2021). Figure S8 shows that BrC in the gas phase had a moderate good positive
342 correlation ($r=0.4$) with temperature. This explains why the temperature shows a similar diurnal profile as the gas-
343 phase BrC. Therefore, particle-to-gas partitioning was also an important source for gas-phase BrC. However, our
344 results are not consistent with previous studies where 16 BrC molecules in gas phase were mainly from primary
345 emission during the biomass burning evenings and secondary formation during the clear days in rural China (Salvador
346 et al., 2021). Our measurement site was several km away from biomass burning sites with ~7-10 km. And the 31
347 potential BrC in the gas-phase sum up to 8.5 ± 6.7 ~~6.2 ± 5.0~~ ng m⁻³, significantly lower than 1720 ng m⁻³ of 16 BrC
348 (Salvador et al., 2021). Cheng et al. (2021) found that secondary formation was a strong source for five BrC molecules
349 in the gas-phase. Therefore, BrC in the gas-phase are less influenced from primary emissions from biomass burning
350 but are mainly controlled by secondary formation and partitioning in rural Germany.

351 **3.5 Diurnal variations and sources of potential BrC in the particle phase**

352 The 178 potential BrC molecules in the particle phase (PBrC) exhibited two peaks in the diurnal profile (Figure 3a4a)
353 averaged over the whole winter campaign. They increased from 19:00 to 01:00 with a peak at 82 ± 35 ng m⁻³ around
354 midnight. Then the PBrC slowly decreased after midnight. However, they increased again from 6:00 to 08:00 and
355 forming a second peak with 10276 ± 4950 ng m⁻³ in the morning. During daytime, they decreased reaching lowest
356 values with 6147 ± 3124 ng m⁻³ at 14:00-15:00. During the nighttime and morning hours, the higher mass

357 concentrations of PBrC were caused by residential wood burning emissions. Consistently, higher PM_{2.5} concentration
358 levels at nighttime at a rural site near Karlsruhe, Germany, could be assigned to wood burning emissions from wood
359 stove operation during winter (Thieringer et al., 2022). The low mass concentrations of PBrC at daytime could be
360 explained by photobleaching and evaporation of BrC, and/or dilution by the increasing planetary boundary layer
361 heights (Satish et al., 2017). Satish et al. (2017) found that BrC over the Indo-Gangetic Plain had two peaks of BrC at
362 evening and morning hours, and lowest values during daytime.

363 To determine the sources of brown carbon, we used the edge approach (Day et al., 2015). It allows to estimate the
364 contribution of primary biomass burning (BB) to the measured BrC concentrations using levoglucosan as a primary
365 source tracer. This approach is analogous to the widely used elemental carbon (EC) tracer approach, in which EC is
366 used to distinguish the primary organic carbon (POC) and secondary organic carbon (SOC) in total organic carbon
367 (OC) measurements (Day et al., 2015; Cabada et al., 2004). Levoglucosan (lev) and potential BrC were measured
368 online by the same instruments and under the same conditions. As discussed above, we observed a good correlation
369 (r=0.8) between levoglucosan and BC during the winter campaign. Therefore, levoglucosan is a suitable tracer for
370 primary BB. Please note that we did not calibrate the sensitivities of levoglucosan detected by FIGAERO-CIMS.
371 Therefore, it could cause some uncertainties to estimate brown carbon from biomass burning and secondary formation.
372 Figure 4a-5a shows that the blue points can be used as edge points to determine the ratio of BrC/levoglucosan at the
373 primary emissions from biomass burning. The relative contributions of primary emissions (BB) and secondary (sec)
374 formation for total BrC molecules were estimated using the following expression:

$$375 \quad BrC_{BB} = \left(\frac{[BrC]}{[lev]_{BB}} \right) * [lev.]$$

$$376 \quad [BrC_{sec}] = [BrC_{Tot}] - [BrC_{BB}]$$

377 Where $([BrC]/[lev])_{BB}$ is the ratio of the concentration of the BrC to that of levoglucosan in the primary emissions from
378 biomass burning and this value is 1.19 ± 0.1 (Figure 4a5a), BrC_{BB} and BrC_{sec} are the fractions of BrC generated through
379 biomass burning and secondary production, respectively, BrC_{Tot} and lev. are the measured concentrations of BrC and
380 levoglucosan during the winter campaign. Using this approach, we calculated the diurnal profiles of BrC from primary
381 emissions (BrC_{BB}) and secondary formation (BrC_{sec}) shown in Figure 4b5b. The uncertainty of the splitting between
382 BrC from biomass burning and of secondary origin is mainly based on the levoglucosan concentration for which we
383 have included the calibration. Based on this we estimated the uncertainty of the BrC source splitting to $\pm 35\%$. The

384 mass fraction of BrC_{sec} increased at daytime and decreased at evening. This indicates that the secondary formation for
385 BrC in the particle phase was enhanced during daytime, facilitated by the higher levels of oxidants e.g. O₃ (Figure
386 ~~3e4c~~). The mass fraction of BrC_{BB} had two peaks at early morning and in the evening hours, respectively. This may be
387 caused by residential wood burning emissions. BrC_{BB} accounts for $39 \pm 21\%$ of the total BrC as averaged for the whole
388 measurement period. During biomass burning events, the BrC_{BB} is a major mass fraction for total BrC that accounts
389 for $61 \pm 13\%$ during BB-event1 and $65 \pm 12\%$ during BB-event-2, respectively. Therefore, the primary emissions of
390 BrC have a significant impact on BrC, especially, at biomass burning events. However, on average over the whole
391 campaign, BrC_{sec} dominates the mass fraction of BrC with $61 \pm 21\%$. Therefore, the secondary formation can be
392 considered as an important source for BrC in rural Germany. Consistently, secondary formation from biomass burning
393 emission is important for the brown carbon absorption in the Switzerland, the central Europe. (Moschos et al., 2018).
394 Secondary sources for BrC were more important for absorption than primary ones in the Southeastern Margin of the
395 Tibetan Plateau (Wang et al., 2019b).

396 To further investigate the oxidation of BrC in the particle phase we plotted, the diurnal profiles of O/C ratios of BrC
397 during the whole campaign was measured, as shown in Figure ~~56~~. ~~The O/C ratio of BrC increased at daytime and~~
398 ~~deceased at nighttime. The ozone had the same diurnal profile as the O/C ratio of BrC. The O/C ratio of the potential~~
399 ~~BrC molecules increased during daytime and decreased at nighttime. This is an indication for an impact of photo-~~
400 ~~oxidation on BrC either during formation or aging leading to an increase of its O/C ratio. Consequently, the O/C ratio~~
401 ~~of the potential BrC molecules shows a positive correlation (r=0.8) with ozone, another product of photo chemistry. In~~
402 ~~addition, the O/C ratio of BrC had a positive correlation (r=0.8) with ozone. This indicates that the BrC was photo-~~
403 ~~oxidized leading to an increase of the O/C ratio of BrC.~~ In contrast, the light absorption of BrC at 370 nm ($b_{\text{brc}370}$) and
404 the double bond equivalent (DBE) decreased at daytime and increased at nighttime. During daytime, the absorption of
405 brown carbon at 370 nm decreased due to lower DBE and higher O/C values of brown carbon caused by photooxidation.
406 This is in accordance with previous studies where atmospheric photooxidation diminishes light absorption of primary
407 brown carbon aerosol from biomass burning (Sumlin et al., 2017). Oxidative whitening can reduce light absorption of
408 brown carbon during the day (Hems et al., 2021).

409 **Conclusions**

410 The chemical composition, diurnal variation, and sources of brown carbon aerosol were investigated during February-
411 March 2021 in a rural area, at KIT Campus Nord, a location characteristic for central Europe. The 178 potential brown
412 carbon molecules (including 7 nitro aromatic compounds, NACs) identified in the particle phase contributed on average
413 83 ± 44 63 ± 32 ng m⁻³ and 31 potential brown carbon molecules (including 4 NACs) identified in the gas phase
414 contributed on average 8.5 ± 6.7 6.2 ± 5.0 ng m⁻³ during the whole campaign. During dedicated biomass burning events,
415 potential BrC concentrations in the particle phase were significantly higher with up to ~ 254 ~~100~~ ng m⁻³. The 178
416 identified potential brown carbon molecules only accounted for $2.63 \pm 1.5\%$ of the total organic mass, but explained
417 ~~11~~ 14 ± 11 13% of the total brown carbon absorption at 370 nm, assuming a MAC₃₇₀ as 9.5 m² g⁻¹. This shows that a
418 small fraction of the brown carbon molecules dominates the overall absorption. This indicates the great importance of
419 identifying these molecules, the strong absorbers, to predict aerosol absorption.

420 Diurnal variations show that the particle-phase potential BrC had two peaks at early morning and evening hours,
421 respectively. These were mainly caused by residential wood burning emissions. In contrast, the gas-phase potential
422 BrC showed higher concentrations at daytime and lower concentrations at nighttime. The gas-phase BrC molecules
423 were mainly controlled by secondary formation (e.g. by photochemical processes) and particle-to-gas partitioning. The
424 two main sources contributed to particle-phase BrC were primary emission from biomass burning and secondary
425 formation. Secondary formation, e.g. by photooxidation, is an important source of particle-phase BrC corresponding
426 to increasing O/C ratios of BrC during daytime and a positive correlation (r=0.8) with ozone concentrations. In addition,
427 the DBE of the particle-phase decreased during daytime. This indicates that the absorption of brown carbon at 370 nm
428 decreased due to lower DBE and higher O/C ratio due to the photooxidation of brown carbon. Compared with previous
429 measurements in central Europe (Lukács et al., 2007; Zhang et al., 2020), our study found that secondary formation,
430 e.g., photochemical processes, was an important source for BrC in gas and particle phases. To improve air quality in
431 winter, we need to reduce biomass burning emissions (e.g., regulate wood stoves) but also reduce the precursors to
432 form secondary aerosol. Overall, this study provides good insight into the light absorption, sources, and diurnal
433 variation from real-time observations of brown carbon molecules in central Europe by using mass spectrometry and
434 aethalometer.

435 **Data availability**

436 Data are available upon request to the corresponding author.

437 **Competing interests**

438 At least one of the (co-)authors is a member of the editorial board of Atmospheric Chemistry and Physics

439 **Author contributions**

440 FJ and HS designed the measurement campaign. FJ, LG, JS, and HS performed the experimental work. FJ did

441 FIGAERO-CIMS and AE33 data analysis. HS and HZ processed the trace gas and meteorological data, respectively.

442 TL gave general comments for this paper. FJ wrote the paper with contributions from all co-authors.

443 **ACKNOWLEDGMENTS**

444 The authors gratefully thank the staff of IMK-AAF for providing substantial technical support during the field

445 campaigns under COVID conditions. Furthermore, Feng Jiang and Junwei Song are thankful for the support from the

446 China Scholarship Council (CSC).

447

448 REFERENCES

449 Andreae, M. O., and Gelencser, A.: Black carbon or brown carbon? The nature of light-absorbing carbonaceous
450 aerosols, *Atmos. Chem. Phys.* 6, 3131-3148, <https://doi.org/10.5194/acp-6-3131-2006>, 2006.

451 Cabada, J. C., Pandis, S. N., Subramanian, R., Robinson, A. L., Polidori, A., and Turpin, B.: Estimating the secondary
452 organic aerosol contribution to PM_{2.5} using the EC tracer method, *Aerosol Sci. Technol.* 38, 140-155,
453 <https://doi.org/10.1080/02786820390229084>, 2004.

454 Chen, Q. C., Chen, Q., Hua, X. Y., Guan, D. J., and Chang, T.: Gas-phase brown carbon: Absorbance and chromophore
455 types, *Atmos. Environ.* 264, <https://doi.org/10.1016/j.atmosenv.2021.118646>, 2021.

456 Cheng, X., Chen, Q., Li, Y., Huang, G., Liu, Y., Lu, S., Zheng, Y., Qiu, W., Lu, K., Qiu, X., Bianchi, F., Yan, C.,
457 Yuan, B., Shao, M., Wang, Z., Canagaratna, M. R., Zhu, T., Wu, Y., and Zeng, L.: Secondary Production of Gaseous
458 Nitrated Phenols in Polluted Urban Environments, *Environ. Sci. Technol.* 55, 4410-4419,
459 <https://doi.org/10.1021/acs.est.0c07988>, 2021.

460 Daumit, K. E., Kessler, S. H., and Kroll, J. H.: Average chemical properties and potential formation pathways of highly
461 oxidized organic aerosol, *Farad. Disc.* 165, 181-202, <https://doi.org/10.1039/c3fd00045a>, 2013.

462 Day, M. C., Zhang, M. H., and Pandis, S. N.: Evaluation of the ability of the EC tracer method to estimate secondary
463 organic carbon, *Atmos. Environ.* 112, 317-325, <https://doi.org/10.1016/j.atmosenv.2015.04.044>, 2015.

464 Donahue, N. M., Robinson, A. L., and Pandis, S. N.: Atmospheric organic particulate matter: From smoke to secondary
465 organic aerosol, *Atmos. Environ.* 43, 94-106, <https://doi.org/10.1016/j.atmosenv.2008.09.055>, 2009.

466 Drinovec, L., Mocnik, G., Zotter, P., Prevot, A. S. H., Ruckstuhl, C., Coz, E., Rupakheti, M., Sciare, J., Muller, T.,
467 Wiedensohler, A., and Hansen, A. D. A.: The "dual-spot" Aethalometer: an improved measurement of aerosol black
468 carbon with real-time loading compensation, *Atmos. Meas. Tech.* 8, 1965-1979, [https://doi.org/10.5194/amt-8-1965-](https://doi.org/10.5194/amt-8-1965-2015)
469 2015, 2015.

470 [Duan, Jing, Ru-Jin Huang, Chunshui Lin, Jincan Shen, Lu Yang, Wei Yuan, Ying Wang, Yi Liu, and Wei Xu.:
471 Aromatic Nitration Enhances Absorption of Biomass Burning Brown Carbon in an Oxidizing Urban Environment,
472 Environ. Sci. Technol., 58, 17344-54, https://doi.org/10.1021/acs.est.4c05558, 2024.](#)

473 [Drinovec, L., G. Mocnik, P. Zotter, A. S. H. Prevot, C. Ruckstuhl, E. Coz, M. Rupakheti, J. Sciare, T. Muller, A.
474 Wiedensohler, and A. D. A. Hansen.: The "dual-spot" Aethalometer: an improved measurement of aerosol black carbon
475 with real-time loading compensation, Atmos. Meas. Tech., 8, 1965-79, https://doi.org/10.5194/amt-8-1965-2015, 2015.](#)

476 Gundel, L. A., Dod, R. L., Rosen, H., and Novakov, T.: The relationship between optical attenuation and black carbon
477 concentration for ambient and source particles, *Sci. Total Environ.* 36, 197-202, [https://doi.org/10.1016/0048-](https://doi.org/10.1016/0048-9697(84)90266-3)
478 9697(84)90266-3, 1984.

479 [Healy, R. M., U. Sofowote, Y. Su, J. Deboz, M. Noble, C. H. Jeong, J. M. Wang, N. Hilker, G. J. Evans, G. Doerksen,](#)
480 [K. Jones, and A. Munoz.: Ambient measurements and source apportionment of fossil fuel and biomass burning black](#)
481 [carbon in Ontario, Atmos. Environ., 161, 34-47, <https://doi.org/10.1016/j.atmosenv.2017.04.034>, 2017.](#)

482 [Helin, Aku, Jarkko V. Niemi, Aki Virkkula, Liisa Pirjola, Kimmo Teinilä, John Backman, Minna Aurela, Sanna](#)
483 [Saarikoski, Topi Rönkkö, Eija Asmi, and Hilka Timonen.: Characteristics and source apportionment of black carbon](#)
484 [in the Helsinki metropolitan area, Finland, Atmos. Environ., 190, 87-98,](#)
485 <https://doi.org/10.1016/j.atmosenv.2018.07.022>, 2018.

486 Hems, R. F., Schnitzler, E. G., Liu-Kang, C., Cappa, C. D., and Abbatt, J. P. D.: Aging of Atmospheric Brown Carbon
487 Aerosol, ACS Earth Space Chem. 5, 722-748, <https://doi.org/10.1021/acsearthspacechem.0c00346>, 2021.

488 Huang, R.-J., Yang, L., Cao, J., Chen, Y., Chen, Q., Li, Y., Duan, J., Zhu, C., Dai, W., Wang, K., Lin, C., Ni, H.,
489 Corbin, J. C., Wu, Y., Zhang, R., Tie, X., Hoffmann, T., O'Dowd, C., and Dusek, U.: Brown Carbon Aerosol in Urban
490 Xi'an, Northwest China: The Composition and Light Absorption Properties, Environ. Sci. Technol. 52, 6825-6833,
491 <https://doi.org/10.1021/acs.est.8b02386>, 2018.

492 [Huang, Wei, Harald Saathoff, Aki Pajunoja, Xiaoli Shen, Karl-Heinz Naumann, Robert Wagner, Annele Virtanen,](#)
493 [Thomas Leisner, and Claudia Mohr.: alpha-Pinene secondary organic aerosol at low temperature: chemical](#)
494 [composition and implications for particle viscosity, Atmos. Chem. Phys., 18, 2883-98, \[https://doi.org/10.5194/acp-18-\]\(https://doi.org/10.5194/acp-18-2883-2018\)](#)
495 [2883-2018](https://doi.org/10.5194/acp-18-2883-2018), 2018.

496 Huang, W., Saathoff, H., Shen, X., Ramisetty, R., Leisner, T., and Mohr, C.: Chemical Characterization of Highly
497 Functionalized Organonitrates Contributing to Night-Time Organic Aerosol Mass Loadings and Particle Growth,
498 Environ. Sci. Technol. 53, 1165-1174, <https://doi.org/10.1021/acs.est.8b05826>, 2019a.

499 Huang, W., Saathoff, H., Shen, X. L., Ramisetty, R., Leisner, T., and Mohr, C.: Seasonal characteristics of organic
500 aerosol chemical composition and volatility in Stuttgart, Germany, Atmos. Chem. Phys. 19, 11687-11700,
501 <https://doi.org/10.5194/acp-19-11687-2019>, 2019b.

502 Jiang, F., Song, J. W., Bauer, J., Gao, L. Y., Vallon, M., Gebhardt, R., Leisner, T., Norra, S., and Saathoff, H.:
503 Chromophores and chemical composition of brown carbon characterized at an urban kerbside by excitation-emission
504 spectroscopy and mass spectrometry, Atmos. Chem. Phys. 22, 14971-14986, [https://doi.org/10.5194/acp-22-14971-](https://doi.org/10.5194/acp-22-14971-2022)
505 [2022](https://doi.org/10.5194/acp-22-14971-2022), 2022.

506 Jiang, F., Siemens, K., Linke, C., Li, Y., Gong, Y., Leisner, T., Laskin, A., and Saathoff, H.: Molecular analysis of
507 secondary organic aerosol and brown carbon from the oxidation of indole. Atmos. Chem. Phys. 24(4), 2639-2649.
508 <https://doi.org/10.5194/acp-24-2639-2024>, 2024.

509 [Lack, D. A., and J. M. Langridge. 2013. 'On the attribution of black and brown carbon light absorption using the](#)
510 [Ångström exponent', Atmos. Chem. Phys., 13, 10535-43, <https://doi.org/10.5194/acp-13-10535-2013>, 2013.](#)

511 Laskin, A., Laskin, J., and Nizkorodov, S. A.: Chemistry of Atmospheric Brown Carbon, *Chem. Rev.* 115, 4335-4382,
512 <https://doi.org/10.1021/cr5006167>, 2015.

513 Lee, B., Lopez-Hilfiker, F. D., D'Ambro, E. L., Zhou, P. T., Boy, M., Petaja, T., Hao, L. Q., Virtanen, A., and Thornton,
514 J. A.: Semi-volatile and highly oxygenated gaseous and particulate organic compounds observed above a boreal forest
515 canopy, *Atmos. Chem. Phys.* 11547-11562, <https://doi.org/10.5194/acp-18-11547-2018>, 2018.

516 Lin, P., Liu, J., Shilling, J. E., Kathmann, S. M., Laskin, J., and Laskin, A.: Molecular characterization of brown carbon
517 (BrC) chromophores in secondary organic aerosol generated from photo-oxidation of toluene, *Phys. Chem. Chem.*
518 *Phys.* 17, 23312-23325, <https://doi.org/10.1039/c5cp02563j>, 2015.

519 [Lin, P., P. K. Aiona, Y. Li, M. Shiraiwa, J. Laskin, S. A. Nizkorodov, and A. Laskin.: Molecular Characterization of](https://doi.org/10.1021/acs.est.6b03024)
520 [Brown Carbon in Biomass Burning Aerosol Particles, *Environ. Sci. Technol.*, 50, 11815-24,](https://doi.org/10.1021/acs.est.6b03024)
521 <https://doi.org/10.1021/acs.est.6b03024>, 2016.

522 [Lin, P., L. T. Fleming, S. A. Nizkorodov, J. Laskin, and A. Laskin.: Comprehensive Molecular Characterization of](https://doi.org/10.1021/acs.analchem.8b02177)
523 [Atmospheric Brown Carbon by High Resolution Mass Spectrometry with Electrospray and Atmospheric Pressure](https://doi.org/10.1021/acs.analchem.8b02177)
524 [Photoionization, *Anal. Chem.*, 90, 12493-502, https://doi.org/10.1021/acs.analchem.8b02177, 2018.](https://doi.org/10.1021/acs.analchem.8b02177)

525 [Linke, C., I. Ibrahim, N. Schleicher, R. Hitzenberger, M. O. Andreae, T. Leisner, and M. Schnaiter.: A novel single-](https://doi.org/10.5194/amt-9-5331-2016)
526 [cavity three-wavelength photoacoustic spectrometer for atmospheric aerosol research, *Atmos. Meas. Tech.*, 9, 5331-](https://doi.org/10.5194/amt-9-5331-2016)
527 [46, https://doi.org/10.5194/amt-9-5331-2016, 2016.](https://doi.org/10.5194/amt-9-5331-2016)

528 Liu, X., Wang, H., Wang, F., Lv, S., Wu, C., Zhao, Y., Zhang, S., Liu, S., Xu, X., Lei, Y., and Wang, G.: Secondary
529 Formation of Atmospheric Brown Carbon in China Haze: Implication for an Enhancing Role of Ammonia, *Environ.*
530 *Sci. Technol.* 57, 11163-11172, <https://doi.org/10.1021/acs.est.3c03948>, 2023.

531 Lukács, H., Gelencsér, A., Hammer, S., Puxbaum, H., Pio, C., Legrand, M., Kasper-Giebl, A., Handler, M., Limbeck,
532 A., Simpson, D., and Preunkert, S.: Seasonal trends and possible sources of brown carbon based on 2-year aerosol
533 measurements at six sites in Europe, *J. Geophys. Res.* 112, <https://doi.org/10.1029/2006JD008151>, 2007.

534 Lopez-Hilfiker, F. D., Mohr, C., Ehn, M., Rubach, F., Kleist, E., Wildt, J., Mentel, T. F., Lutz, A., Hallquist, M.,
535 Worsnop, D., and Thornton, J. A.: A novel method for online analysis of gas and particle composition: description and
536 evaluation of a Filter Inlet for Gases and AEROSols (FIGAERO), *Atmos. Meas. Tech.* 7, 983-1001,
537 <https://doi.org/10.5194/amt-7-983-2014>, 2014.

538 [Lopez-Hilfiker, F. D., S. Iyer, C. Mohr, B. H. Lee, E. L. D'Ambro, T. Kurten, and J. A. Thornton. 2016.: Constraining](https://doi.org/10.5194/amt-9-1505-2016)
539 [the sensitivity of iodide adduct chemical ionization mass spectrometry to multifunctional organic molecules using the](https://doi.org/10.5194/amt-9-1505-2016)
540 [collision limit and thermodynamic stability of iodide ion adducts, *Atmos. Meas. Tech.*, 9, 1505-12,](https://doi.org/10.5194/amt-9-1505-2016)
541 [https://doi.org/10.5194/amt-9-1505-2016, 2016.](https://doi.org/10.5194/amt-9-1505-2016)

542 Mohr, C., Lopez-Hilfiker, F. D., Zotter, P., Prevot, A. S. H., Xu, L., Ng, N. L., Herndon, S. C., Williams, L. R., Franklin,
543 J. P., Zahniser, M. S., Worsnop, D. R., Knighton, W. B., Aiken, A. C., Gorkowski, K. J., Dubey, M. K., Allan, J. D.,
544 and Thornton, J. A.: Contribution of Nitrated Phenols to Wood Burning Brown Carbon Light Absorption in Detling,
545 United Kingdom during Winter Time, *Environ. Sci. Technol.* 47, 6316-6324, <https://doi.org/10.1021/es400683v>, 2013.

546 Moise, T., Flores, J. M., and Rudich, Y.: Optical Properties of Secondary Organic Aerosols and Their Changes by
547 Chemical Processes, *Chem. Rev.* 115, 4400-4439, <https://doi.org/10.1021/cr5005259>, 2015.

548 Montoya-Aguilera, J., Horne, J. R., Hinks, M. L., Fleming, L. T., Perraud, V., Lin, P., Laskin, A., Laskin, J., Dabdub,
549 D., and Nizkorodov, S. A.: Secondary organic aerosol from atmospheric photooxidation of indole, *Atmos. Chem. Phys.*
550 17, 11605-11621, <https://doi.org/10.5194/acp-17-11605-2017>, 2017.

551 Moschos, V., Kumar, N. K., Daellenbach, K. R., Baltensperger, U., Prevot, A. S. H., and El Haddad, I.: Source
552 Apportionment of Brown Carbon Absorption by Coupling Ultraviolet-Visible Spectroscopy with Aerosol Mass
553 Spectrometry, *Environ. Sci. Tech. Lett.* 5, 302-+, <https://doi.org/10.1021/acs.estlett.8b00118>, 2018.

554 Moschos, V., Gysel-Beer, M., Modini, R. L., Corbin, J. C., Massabo, D., Costa, C., Danelli, S. G., Vlachou, A.,
555 Daellenbach, K. R., Szidat, S., Prati, P., Prevot, A. S. H., Baltensperger, U., and El Haddad, I.: Source-specific light
556 absorption by carbonaceous components in the complex aerosol matrix from yearly filter-based measurements, *Atmos.*
557 *Chem. Phys.* 21, 12809-12833, <https://doi.org/10.5194/acp-21-12809-2021>, 2021.

558 Palm, B. B., Peng, Q. Y., Fredrickson, C. D., Lee, B., Garofalo, L. A., Pothier, M. A., Kreidenweis, S. M., Farmer, D.
559 K., Pokhrel, R. P., Shen, Y. J., Murphy, S. M., Permar, W., Hu, L., Campos, T. L., Hall, S. R., Ullmann, K., Zhang,
560 X., Flocke, F., Fischer, E. V., and Thornton, J. A.: Quantification of organic aerosol and brown carbon evolution in
561 fresh wildfire plumes, *P. Natl. Acad. Sci. USA.* 117, 29469-29477, <https://doi.org/10.1073/pnas.2012218117>, 2020.

562 Park, R. J., Kim, M. J., Jeong, J. I., Youn, D., and Kim, S.: A contribution of brown carbon aerosol to the aerosol light
563 absorption and its radiative forcing in East Asia, *Atmos. Environ.* 44, 1414-1421,
564 <https://doi.org/10.1016/j.atmosenv.2010.01.042>, 2010.

565 Saarikoski, S., Niemi, J. V., Aurela, M., Pirjola, L., Kousa, A., Ronkko, T., and Timonen, H.: Sources of black carbon
566 at residential and traffic environments obtained by two source apportionment methods, *Atmos. Chem. Phys.* 21, 14851-
567 14869, <https://doi.org/10.5194/acp-21-14851-2021>, 2021.

568 [Saathoff, H., K. H. Naumann, M. Schnaiter, W. Schöck, O. Möhler, U. Schurath, E. Weingartner, M. Gysel, and U.](#)
569 [Baltensperger.: Coating of soot and \(NH₄\)₂SO₄ particles by ozonolysis products of \$\alpha\$ -pinene, *J. Aerosol Sci.*, 34, 1297-](#)
570 [321, \[https://doi.org/10.1016/S0021-8502\\(03\\)00364-1\]\(https://doi.org/10.1016/S0021-8502\(03\)00364-1\), 2003.](#)

571 Salvador, C. M. G., Tang, R. Z., Priestley, M., Li, L. J., Tsiligiannis, E., Le Breton, M., Zhu, W. F., Zeng, L. M., Wang,
572 H., Yu, Y., Hu, M., Guo, S., and Hallquist, M.: Ambient nitro-aromatic compounds - biomass burning versus secondary
573 formation in rural China, *Atmos. Chem. Phys.* 21, 1389-1406, <https://doi.org/10.5194/acp-21-1389-2021>, 2021.

574 Sandradewi, J., Prevot, A. S. H., Szidat, S., Perron, N., Alfarra, M. R., Lanz, V. A., Weingartner, E., and Baltensperger,
575 U.: Using aerosol light absorption measurements for the quantitative determination of wood burning and traffic
576 emission contributions to particulate matter, *Environ. Sci. Technol.* 42, 3316-3323, <https://doi.org/10.1021/es702253m>,
577 2008a.

578 Sandradewi, J., Prevot, A. S. H., Weingartner, E., Schmidhauser, R., Gysel, M., and Baltensperger, U.: A study of
579 wood burning and traffic aerosols in an Alpine valley using a multi-wavelength Aethalometer, *Atmos. Environ.* 42,
580 101-112, <https://doi.org/10.1016/j.atmosenv.2007.09.034>, 2008b.

581 Satish, R., Shamjad, P., Thamban, N., Tripathi, S., and Rastogi, N.: Temporal Characteristics of Brown Carbon over
582 the Central Indo-Gangetic Plain, *Environ. Sci. Technol.* 51, 6765-6772, <https://doi.org/10.1021/acs.est.7b00734>, 2017.

583 Shen, X. L., Vogel, H., Vogel, B., Huang, W., Mohr, C., Ramisetty, R., Leisner, T., Prévôt, A. S. H., and Saathoff, H.:
584 Composition and origin of PM_{2.5} aerosol particles in the upper Rhine valley in summer. *Atmos. Chem. Phys.* 19,
585 13189-13208. <https://doi.org/10.5194/acp-19-13189-2019>, 2019.

586 Siemens, K., Morales, A., He, Q., Li, C., Hettiyadura, A. P. S., Rudich, Y., and Laskin, A.: Molecular Analysis of
587 Secondary Brown Carbon Produced from the Photooxidation of Naphthalene, *Environ. Sci. Technol.*, 56, 3340-3353,
588 <https://doi.org/10.1021/acs.est.1c03135>, 2022.

589 [Song, J., H. Saathoff, F. Jiang, L. Gao, H. Zhang, and T. Leisner.: Sources of organic gases and aerosol particles and](#)
590 [their roles in nighttime particle growth at a rural forested site in southwest Germany, *Atmos. Chem. Phys.*, 24, 6699-](#)
591 [717, <https://doi.org/10.5194/acp-24-6699-2024>, 2024.](#)

592 Song, J. W., Saathoff, H., Gao, L. Y., Gebhardt, R., Jiang, F., Vallon, M., Bauer, J., Norra, S., and Leisner, T.:
593 Variations of PM_{2.5} sources in the context of meteorology and seasonality at an urban street canyon in Southwest
594 Germany, *Atmos. Environ.* 282, <https://doi.org/10.1016/j.atmosenv.2022.119147>, 2022.

595 Sumlin, B. J., Pandey, A., Walker, M. J., Pattison, R. S., Williams, B. J., and Chakrabarty, R. K.: Atmospheric
596 Photooxidation Diminishes Light Absorption by Primary Brown Carbon Aerosol from Biomass Burning, *Environ. Sci.*
597 *Technol. Lett.* 4, 540-545, <https://doi.org/10.1021/acs.estlett.7b00393>, 2017.

598 [Tang, J., Li, J., Su, T., Han, Y., Mo, Y. Z., Jiang, H. X., Cui, M., Jiang, B., Chen, Y. J., Tang, J. H., Song, J. Z., Peng,](#)
599 [P. A., and Zhang, G.: Molecular compositions and optical properties of dissolved brown carbon in biomass burning,](#)
600 [coal combustion, and vehicle emission aerosols illuminated by excitation-emission matrix spectroscopy and Fourier](#)
601 [transform ion cyclotron resonance mass spectrometry analysis, *Atmos. Chem. Phys.*, 20, 2513–2532,](#)
602 [<https://doi.org/10.5194/acp-20-2513-2020>, 2020.](#)

603 Teich, M., van Pinxteren, D., Kecorius, S., Wang, Z. B., and Herrmann, H.: First Quantification of Imidazoles in
604 Ambient Aerosol Particles: Potential Photosensitizers, Brown Carbon Constituents, and Hazardous Components,
605 *Environ. Sci. Technol.* 50, 1166-1173, <https://doi.org/10.1021/acs.est.5b05474>, 2016.

606 Teich, M., van Pinxteren, D., Wang, M., Kecorius, S., Wang, Z. B., Muller, T., Mocnik, G., and Herrmann, H.:
607 Contributions of nitrated aromatic compounds to the light absorption of water-soluble and particulate brown carbon in
608 different atmospheric environments in Germany and China, *Atmos. Chem. Phys.* 17, 1653-1672,
609 <https://doi.org/10.5194/acp-17-1653-2017>, 2017.

610 Thieringer, J. R. D., Szabadi, J., Meyer, J., and Dittler, A.: Impact of Residential Real-World Wood Stove Operation
611 on Air Quality concerning PM_{2.5} Immission, *Processes*, 10, 545, <https://doi.org/10.3390/pr10030545>, 2022.

612 Thompson, S. L., Yatavelli, R. L. N., Stark, H., Kimmel, J. R., Krechmer, J. E., Day, D. A., Hu, W., Isaacman-
613 VanWertz, G., Yee, L., Goldstein, A. H., Khan, M. A. H., Holzinger, R., Kreisberg, N., Lopez-Hilfiker, F. D., Mohr,
614 C., Thornton, J. A., Jayne, J. T., Canagaratna, M., Worsnop, D. R., and Jimenez, J. L.: Field intercomparison of the
615 gas/particle partitioning of oxygenated organics during the Southern Oxidant and Aerosol Study (SOAS) in 2013,
616 *Aerosol Sci. Technol.* 51, 30-56, <https://doi.org/10.1080/02786826.2016.1254719>, 2017.

617 Wang, Q., Ye, J., Wang, Y., Zhang, T., Ran, W., Wu, Y., Tian, J., Li, L., Zhou, Y., Hang Ho, S. S., Dang, B., Zhang,
618 Q., Zhang, R., Chen, Y., Zhu, C., and Cao, J.: Wintertime Optical Properties of Primary and Secondary Brown Carbon
619 at a Regional Site in the North China Plain, *Environ. Sci. Technol.* <https://doi.org/10.1021/acs.est.9b03406>, 2019a.

620 Wang, Q. Y., Han, Y. M., Ye, J. H., Liu, S. X., Pongpiachan, S., Zhang, N. N., Han, Y. M., Tian, J., Wu, C., Long, X.,
621 Zhang, Q., Zhang, W. Y., Zhao, Z. Z., and Cao, J. J.: High Contribution of Secondary Brown Carbon to Aerosol Light
622 Absorption in the Southeastern Margin of Tibetan Plateau, *Geophys. Res. Lett.* 46, 4962-4970,
623 <https://doi.org/10.1029/2019gl082731>, 2019b.

624 Wu, G., Wan, X., Gao, S., Fu, P., Yin, Y., Li, G., Zhang, G., Kang, S., Ram, K., and Cong, Z.: Humic-like substances
625 (HULIS) in aerosols of central Tibetan Plateau (Nam Co, 4730 m asl): Abundance, light absorption properties and
626 sources, *Environ. Sci. Technol.* 52, 7203–7211, <https://doi.org/10.1021/acs.est.8b01251>, 2018.

627 Xie, M., Chen, X., Hays, M. D., Lewandowski, M., Offenberg, J., Kleindienst, T. E., and Holder, A. L.: Light
628 Absorption of Secondary Organic Aerosol: Composition and Contribution of Nitroaromatic Compounds, *Environ. Sci.*
629 *Technol.* 51, 11607– 11616, <https://doi.org/10.1021/acs.est.7b03263>, 2017.

630 [Xu, J. Z., Hettiyadura, A. P. S., Liu, Y. M., Zhang, X. H., Kang, S. C., and Laskin, A.: Regional Differences of](#)
631 [Chemical Composition and Optical Properties of Aerosols in the Tibetan Plateau, *J. Geophys. Res.-Atmos.*, 125,](#)
632 [e2019JD031226, <https://doi.org/10.1029/2019jd031226>, 2020.](#)

633 Yang, Z., Tsona, N. T., George, C., and Du, L.: Nitrogen-Containing Compounds Enhance Light Absorption of
634 Aromatic-Derived Brown Carbon, *Environ. Sci. Technol.* <https://doi.org/10.1021/acs.est.1c08794>, 2022.

635 [Ye, C., B. Yuan, Y. Lin, Z. Wang, W. Hu, T. Li, W. Chen, C. Wu, C. Wang, S. Huang, J. Qi, B. Wang, C. Wang, W.](#)
636 [Song, X. Wang, E. Zheng, J. E. Krechmer, P. Ye, Z. Zhang, X. Wang, D. R. Worsnop, and M. Shao.: Chemical](#)
637 [characterization of oxygenated organic compounds in the gas phase and particle phase using iodide CIMS with](#)
638 [FIGAERO in urban air, *Atmos. Chem. Phys.*, 21, 8455-78, <https://doi.org/10.5194/acp-21-8455-2021>, 2021.](#)

639 [Yus-Díez, J., V. Bernardoni, G. Močnik, A. Alastuey, D. Ciniglia, M. Ivančič, X. Querol, N. Perez, C. Reche, M.](#)
640 [Rigler, R. Vecchi, S. Valentini, and M. Pandolfi.: Determination of the multiple-scattering correction factor and its](#)
641 [cross-sensitivity to scattering and wavelength dependence for different AE33 Aethalometer filter tapes: a multi-](#)
642 [instrumental approach, Atmos. Meas. Tech., 14: 6335-55, <https://doi.org/10.5194/amt-14-6335-2021>, 2021.](#)

643 Zeng, L. H., Zhang, A. X., Wang, Y. H., Wagner, N. L., Katich, J. M., Schwarz, J. P., Schill, G. P., Brock, C., Froyd,
644 K. D., Murphy, D. M., Williamson, C. J., Kupc, A., Scheuer, E., Dibb, J., and Weber, R. J.: Global Measurements of
645 Brown Carbon and Estimated Direct Radiative Effects, Geophys. Res. Lett. 47, <https://doi.org/10.1029/2020gl088747>,
646 2020.

647 Zhang, Y., Albinet, A., Petit, J.-E., Jacob, V., Chevrier, F., Gille, G., Pontet, S., Chrétien, E., Dominik-Sègue, M.,
648 Levigoureux, G., Močnik, G., Gros, V., Jaffrezo, J.-L., and Favez, O.: Substantial brown carbon emissions from
649 wintertime residential wood burning over France, Sci. Total Environ. 743, 140752,
650 <https://doi.org/10.1016/j.scitotenv.2020.140752>, 2020.

651 [Zotter, P., H. Herich, M. Gysel, I. El-Haddad, Y. Zhang, G. Močnik, C. Hüglin, U. Baltensperger, S. Szidat, and A. S.](#)
652 [H. Prévôt. 2017.: Evaluation of the absorption Ångström exponents for traffic and wood burning in the Aethalometer-](#)
653 [based source apportionment using radiocarbon measurements of ambient aerosol, Atmos. Chem. Phys., 17, 4229-49,](#)
654 [<https://doi.org/10.5194/acp-17-4229-2017>, 2017.](#)

655

656

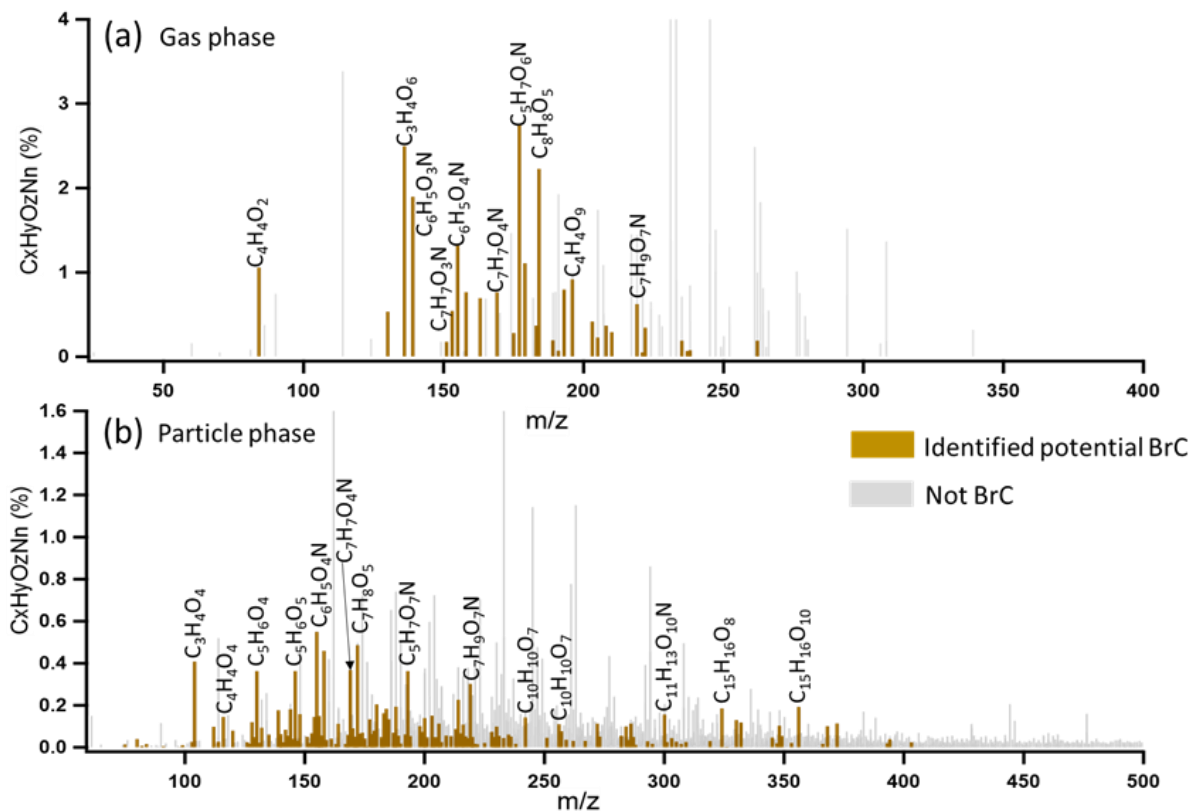
657

658

659

660

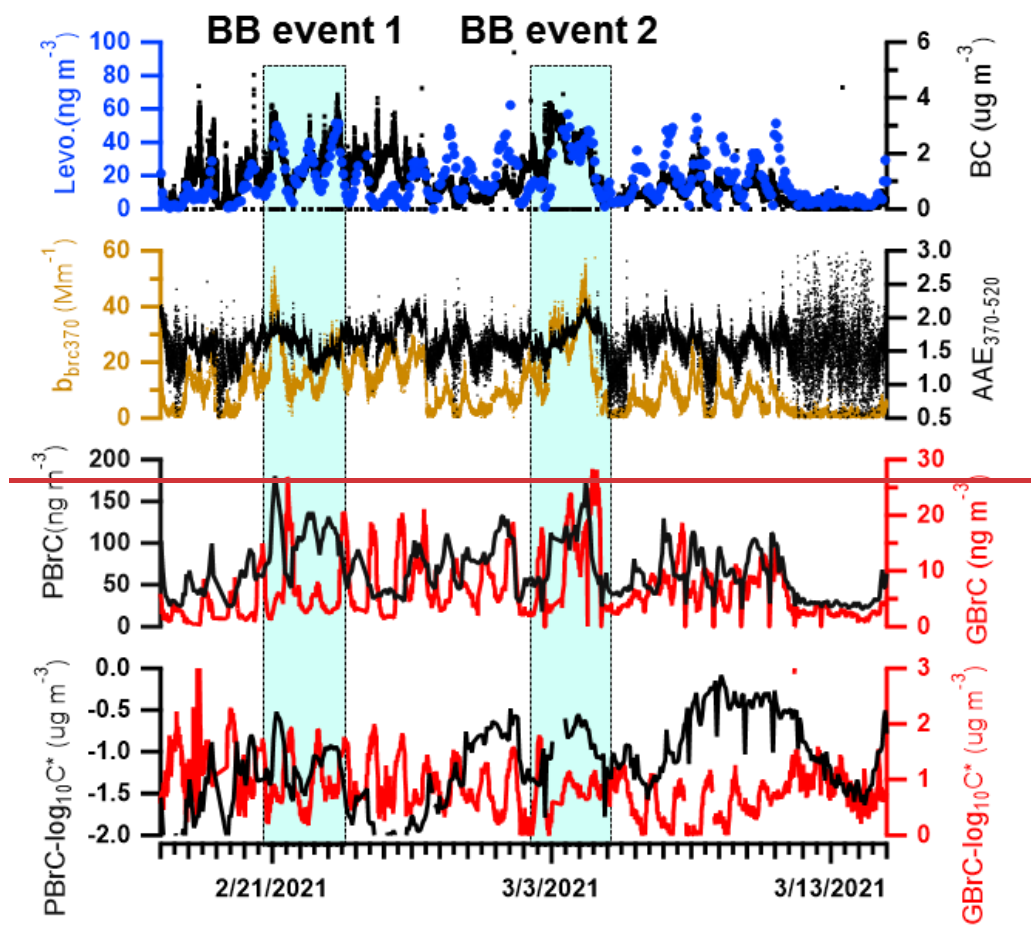
661



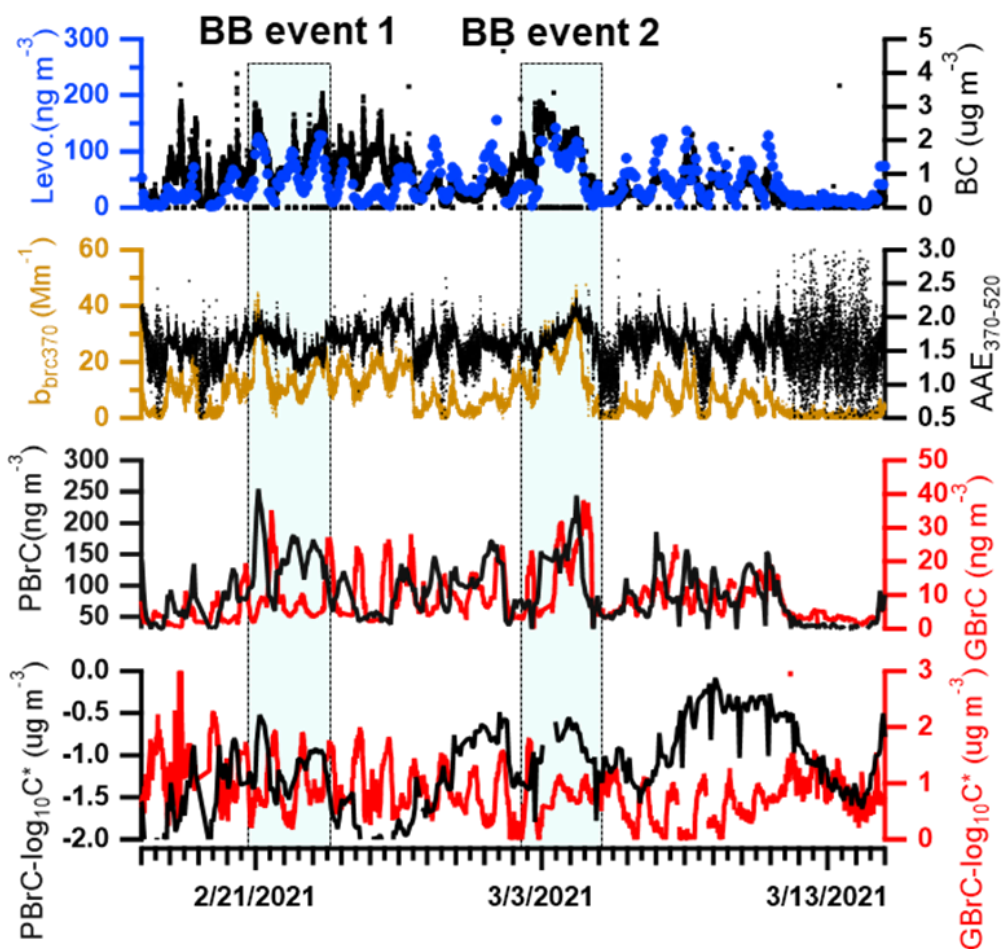
662

663 **Figure 1. CIMS mass spectra of organic aerosol measured by FIGAERO-CIMS for a biomass burning event on**
 664 **March 1st, 2021, a: gas phase, b: particle phase. The CI source employs reactions of I⁻ ions, which convert**
 665 **analyte molecules into [M+I]⁻ ions. Legends above MS features correspond to neutral molecules. The brown**
 666 **peaks in mass spectra were assigned as potential BrC molecules, while the gray peaks refer to the other organic**
 667 **molecules.**

668



669

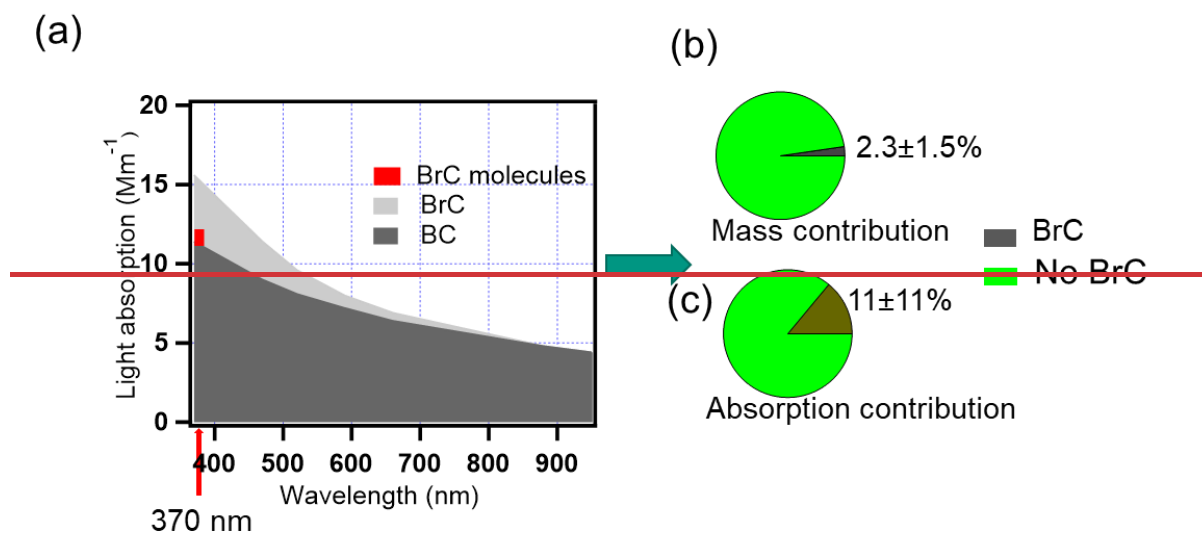


670

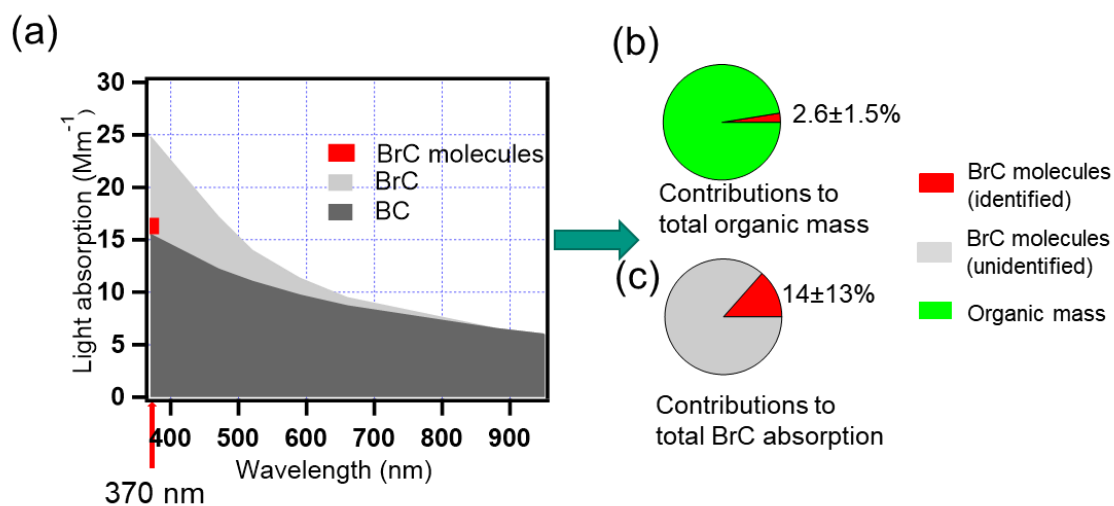
671 **Figure 12.** Time series of levoglucosan (Levo.) concentrations in particle phase from FIGAERO-CIMS, BC
 672 concentrations from aethalometer (AE33), absorption of brown carbon at 370 nm (b_{brc370}), absorption Ångström
 673 exponents between 370 nm and 520 nm ($AAE_{370-520}$), brown carbon concentrations in particle phase (PBrC) and
 674 gas phase (GBrC) and volatility ($\log_{10}C^*$) of brown carbon in particle phase (PBrC_ $\log_{10}C^*$) and gas phase
 675 (GBrC_ $\log_{10}C^*$) during the winter campaign.

676

677



678

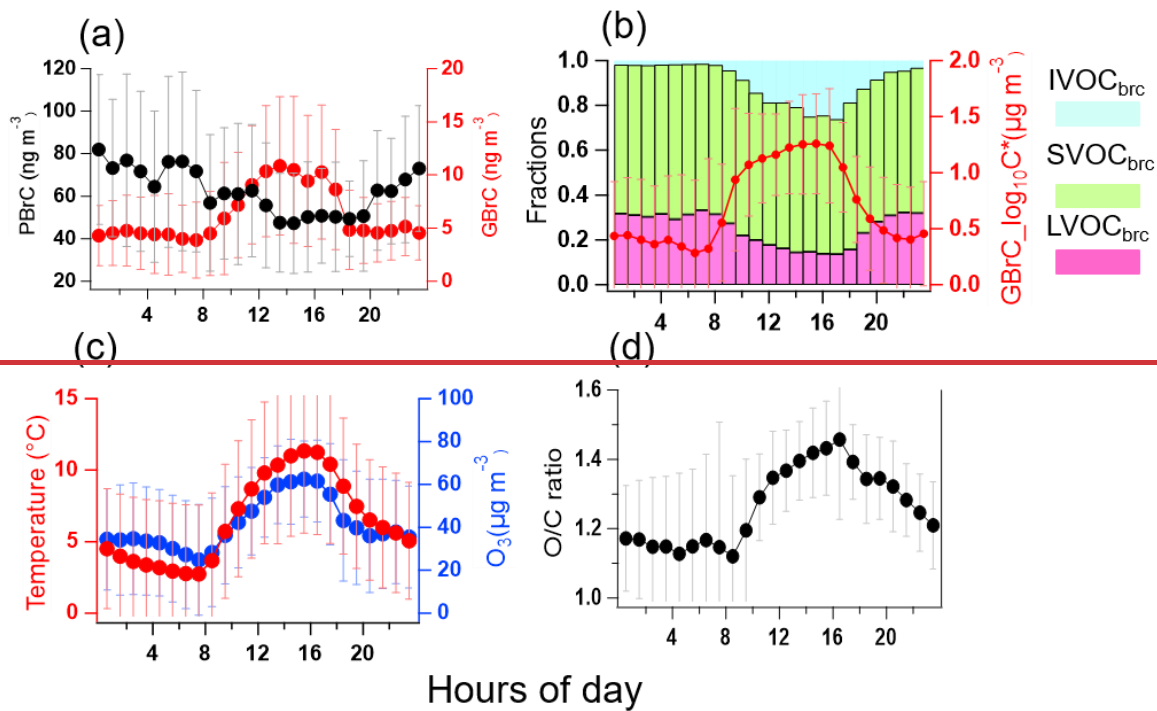


679

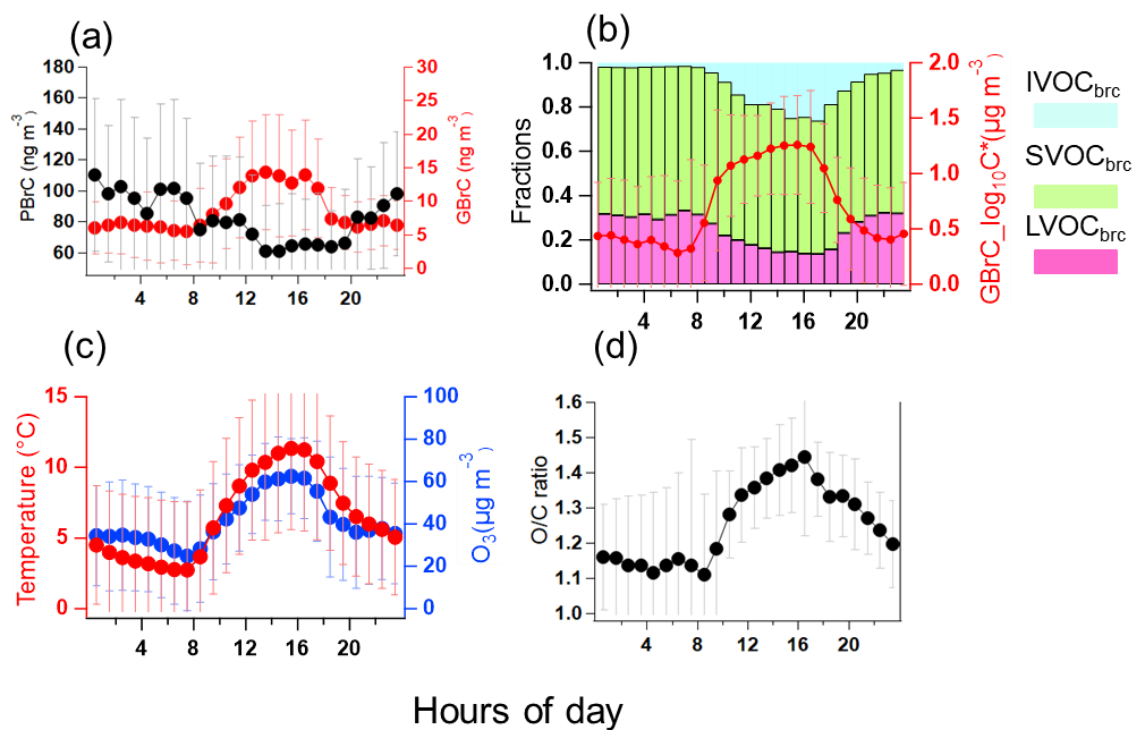
680 **Figure 23.** (a) A stacked plot showing the main contributions to aerosol absorption from brown carbon and
 681 black carbon based on the seven wavelengths measured by the aethalometer AE33. The contribution of the
 682 identified brown carbon molecules to the total aerosol absorption is indicated in red at 370 nm. (b) Average
 683 mass contribution of the potential BrC molecules to estimated total organic mass and (c) absorption contribution
 684 of the potential BrC molecules identified to total absorption by BrC. The green pie: unidentified-BrC; The
 685 red-gray pie: identified BrC molecules; the gray pie: unidentified-BrC molecules; the green pie: all organic mass.

686

687



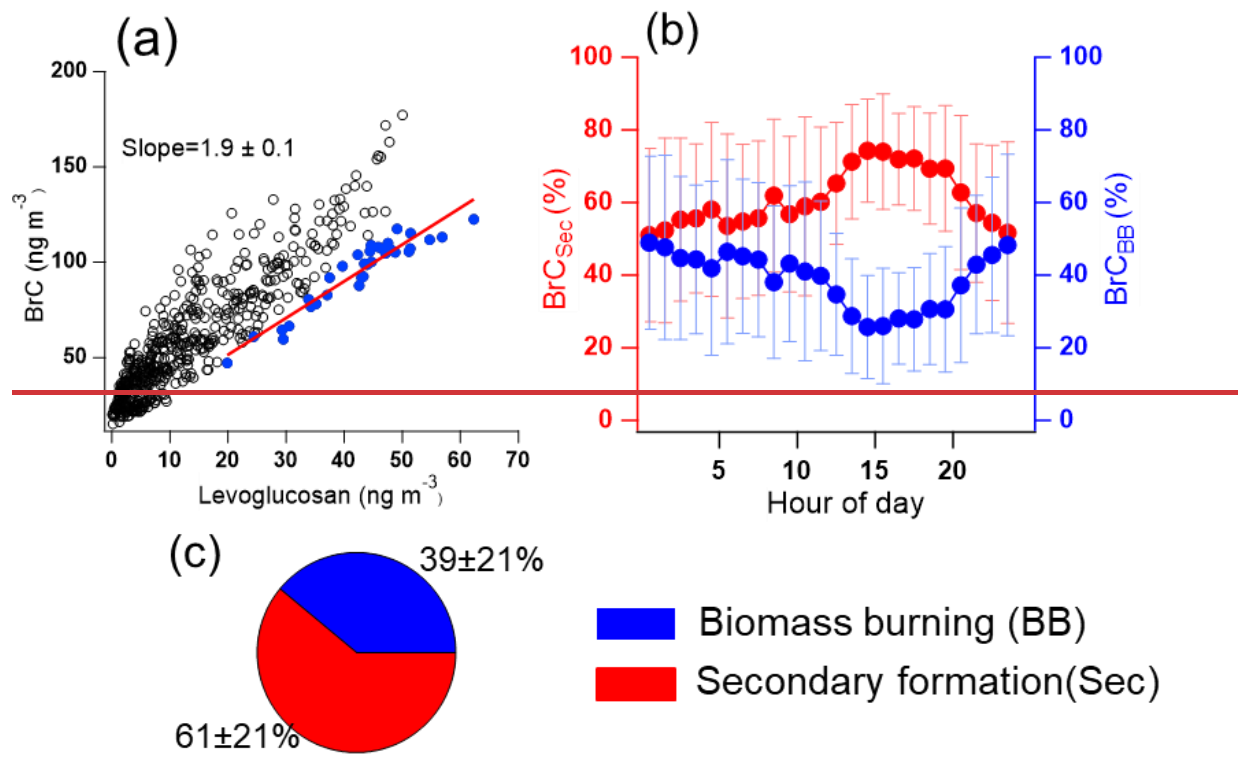
688



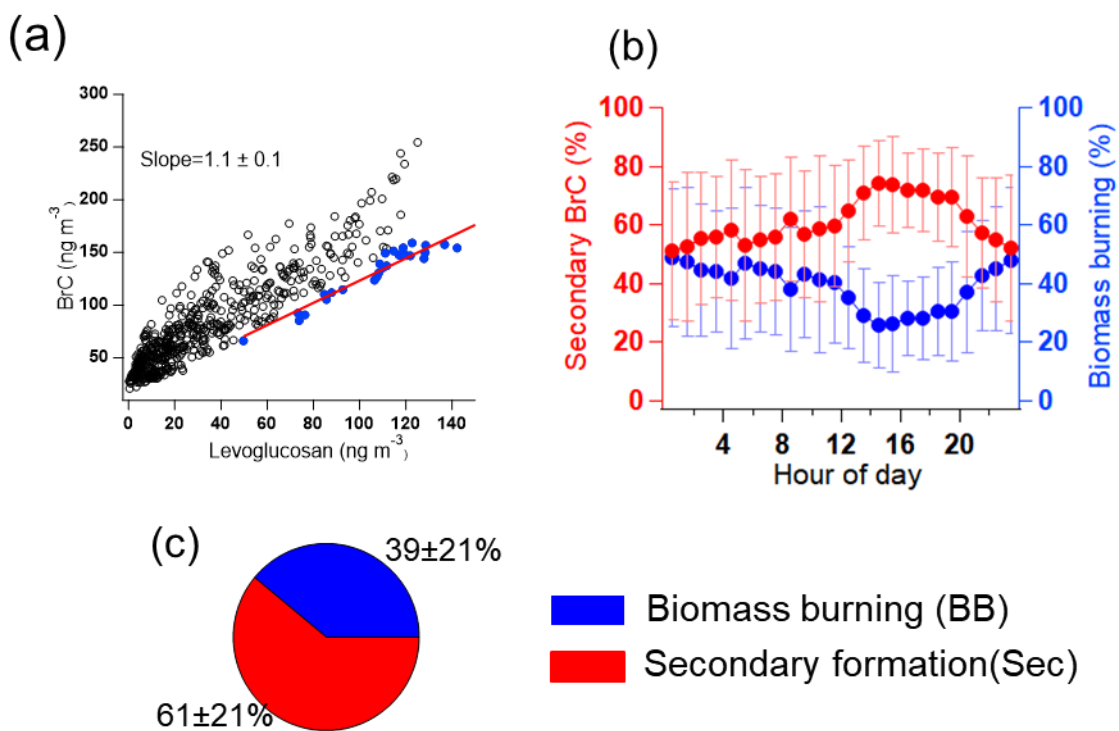
689

690 **Figure 34.** Diurnal profiles averaged over the whole winter campaign of (a) BrC in the particle (PBrC) and gas
 691 phase (GBrC), (b) BrC volatility fractions in LVOC_{brc}, SVOC_{brc}, IVOC_{brc}, and mean BrC volatility in the gas
 692 phase (red line), (c) temperature and ozone concentration. (d) O/C ratio of the oxidized organic components in
 693 the gas phase.

694



696



697

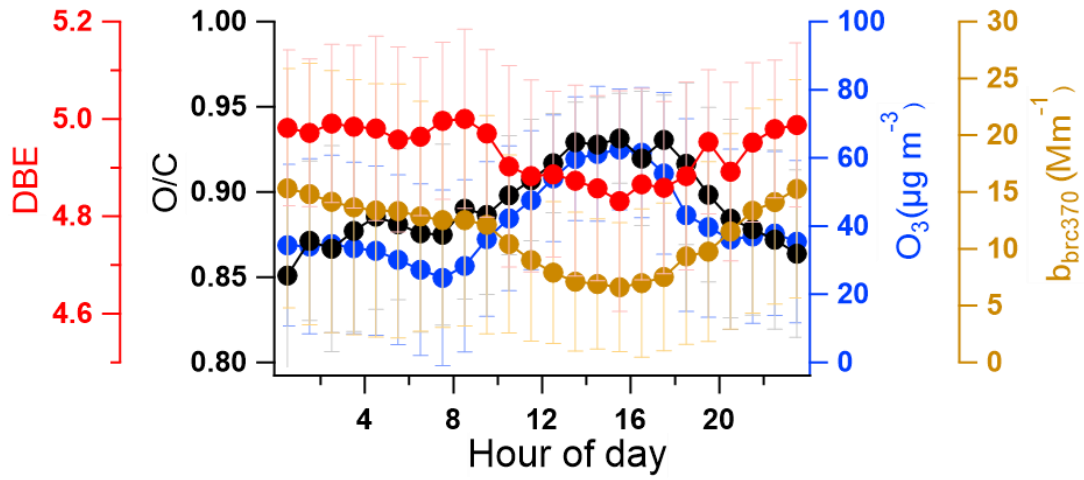
698 **Figure 45.** (a) Correlation analysis of BrC and levoglucosan in the particle phase for the analysis of the
 699 contribution of biomass burning using the edge method (Day et al., 2015). Blue points are the data used to
 700 determine $[\text{BrC}/\text{lev.}]_{\text{BB}}$. (b) diurnal profile of secondary-formation BrC and biomass-burning BrC for the whole

701 **measurement campaign. (c) Average mass fractions of secondary formed BrC and biomass-burning primary**
702 **BrC for the whole campaign.**

703

704

705



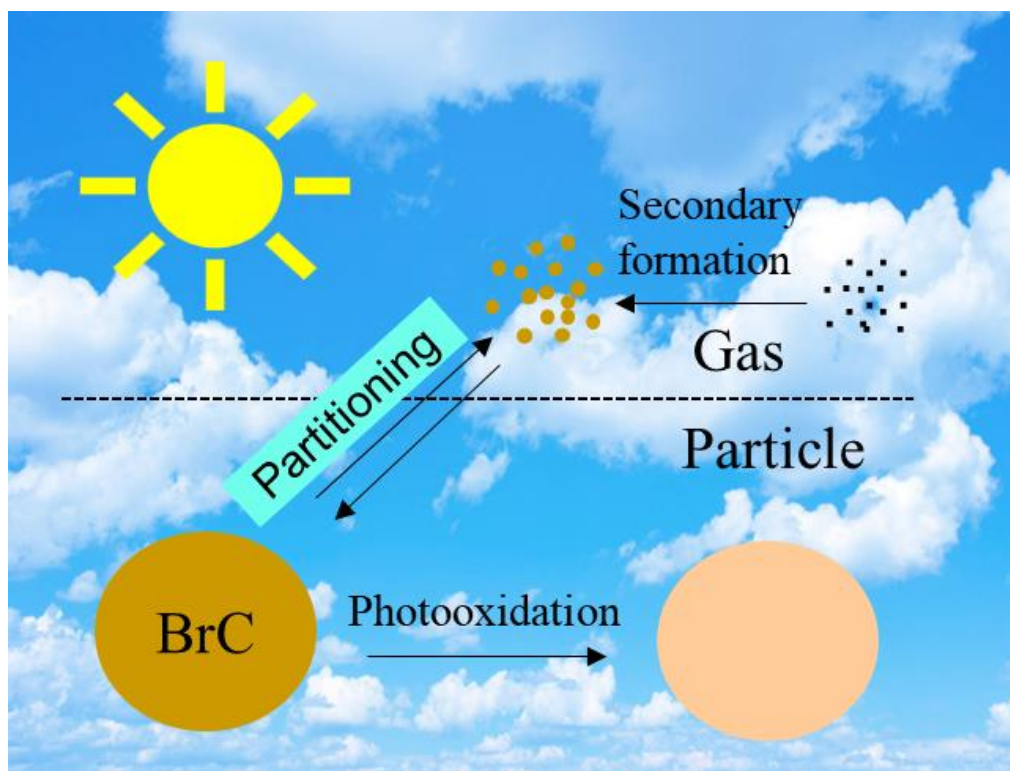
706

707 **Figure 56.** The diurnal profile of DBE (double bond equivalent), O/C ratio of BrC, O₃, and b_{brc370} (absorption
708 of BrC at 370 nm) during the whole measured period.

709

710

711



712

713 **Figure 67.** A conceptual picture of the abstract

714

715

716